Commun. Comput. Phys.
doi: 10.4208/cicp.120715.010216a

Vol. **20**, No. 4, pp. 1045-1070
October 2016

Numerical Analysis of Inverse Elasticity Problem with Signorini's Condition

Cong Zheng[1], Xiaoliang Cheng[1] and Kewei Liang[1,*]

[1] *School of Mathematical Sciences, Zhejiang University, Hangzhou 310027, P.R. China.*

Received 12 July 2015; Accepted (in revised version) 1 February 2016

Abstract. An optimal control problem is considered to find a stable surface traction, which minimizes the discrepancy between a given displacement field and its estimation. Firstly, the inverse elastic problem is constructed by variational inequalities, and a stable approximation of surface traction is obtained with Tikhonov regularization. Then a finite element discretization of the inverse elastic problem is analyzed. Moreover, the error estimation of the numerical solutions is deduced. Finally, a numerical algorithm is detailed and three examples in two-dimensional case illustrate the efficiency of the algorithm.

AMS subject classifications: 65M15, 65N21, 65N22, 74M15, 74S05

Key words: Optimal control, variational inequality, inverse elastic problem, finite element, error estimates, numerical simulations.

1 Introduction

Phenomena of contact between deformable bodies can be observed in daily life and many industries, such as metal forming and metal extrusion, tires with road, braking pads. The vast amounts of engineering literature have studied their mathematical models. Numerous results have been achieved in modelling, mathematical analysis and numerical simulations of contact processes [10, 14, 24]. Recent results of fundamental theories with variational and numerical analysis, including existence and uniqueness results, can be found in [6, 10, 14, 21, 22].

Since the existence, the uniqueness and the stability of the solutions are not always guaranteed [23], almost all of inverse problems are ill-posed problems. For example, the inverse heat transfer problems, which determine the temperatures or heat fluxes on the

*Corresponding author. *Email addresses:* congzheng@zju.edu.cn (C. Zheng), xiaoliangcheng@zju.edu.cn (X. Cheng), matlkw@zju.edu.cn (K. Liang)

 ©2016 Global-Science Press

https://doi.org/10.4208/cicp.120715.010216a Published online by Cambridge University Press

boundary from measured internal temperatures, are very difficult to solve both numerically and analytically [2]. Some strategies have been employed for obtaining proper approximate solutions of inverse problems, such as the least squares method [5,20], regularization [12,13,19,23,25], and dynamic programming [4]. In recent years, the regularization methods are very popular, and they include iterative regularization [13,19], truncated singular value decomposition [12,13] and Tikhonov regularization [12,13,23,25].

For the inverse elastic and elasto-viscoplastic problems, preliminary work with the finite element method and a simple regularization scheme can be found in [15,16]. In [8], authors used a Laplace transform method to solve the boundary temperatures from internal displacements or stresses. In [17,18], researchers utilized a method with boundary integral equations to find plastic strains from surface displacements. Meanwhile, some numerical solutions of an inverse contact problem are given in [11,20]. However, all those papers consider the case of the body force $\boldsymbol{f}_0=\boldsymbol{0}$ and the small displacement observation data $\boldsymbol{u}_d$.

In this paper, the unilateral static contact problem without friction is considered for an elastic body. The aim is to find a stable surface traction $\boldsymbol{p}$ with the given displacement field $\boldsymbol{u}_d$ in the range of the deformation theory of elasticity. We apply the idea of boundary optimal control to formulate this problem. The existence of solution has been proved in [3]. But the uniqueness of the solution can not be guaranteed. The Tikhonov regularization is applied in obtaining a stable approximate solution. Moreover, the adjoint problem of the elastic problem is introduced to construct a feasible numerical algorithm.

The paper is structured as follows. In Section 2, some notations and preliminaries are introduced. The direct problem (DP) of contact problem together with its variational formulation and the uniqueness of solution are displayed in Section 3. In Section 4, the corresponding inverse problem (IP) and the existence of its solution are showed. Meanwhile, the Tikhonov regularization is introduced into the problem to prove the uniqueness of solution, and the convergence of solution is showed. In Section 5, the discrete approximation of the IP is derived by the finite element method. We state the existence and uniqueness of the discrete solution, and derive the error estimates. A simple algorithm is applied to present several numerical simulations of two-dimensional test problem in Section 6. Finally, the summary is presented in Section 7.

2 Notation and preliminaries

In this section, we present the notation to be used throughout the paper (see [10,21,22] for more details). Let $\mathbb{N}$ be the set of all positive integers. We denote by $\mathbb{S}^d$ the space of second order symmetric tensors on $\mathbb{R}^d$, $d\in\mathbb{N}$. The inner product and norm on $\mathbb{R}^d$ and $\mathbb{S}^d$ are defined by

$$\begin{aligned} &\boldsymbol{u}\cdot\boldsymbol{v}=u_iv_i, && \|\boldsymbol{v}\|=(\boldsymbol{v}\cdot\boldsymbol{v})^{\frac{1}{2}}, && \forall\boldsymbol{u},\boldsymbol{v}\in\mathbb{R}^d,\\ &\boldsymbol{\sigma}\cdot\boldsymbol{\tau}=\sigma_{ij}\tau_{ij}, && \|\boldsymbol{\tau}\|=(\boldsymbol{\tau}\cdot\boldsymbol{\tau})^{\frac{1}{2}}, && \forall\boldsymbol{\sigma},\boldsymbol{\tau}\in\mathbb{S}^d. \end{aligned}$$

https://doi.org/10.4208/cicp.120715.010216a Published online by Cambridge University Press

Here and below, the indices i, j, k, l run from 1 to d, unless stated otherwise. The summation convention over repeated indices is used.

Let $\Omega\subset\mathbb{R}^d$ ($d=1,2$ or 3) be a bounded domain with a Lipschitz continuous boundary Γ and let $\boldsymbol{\nu}=(\nu_i)$ the outward unit normal at Γ. We consider a partition of Γ into three disjoint measurable parts Γ_1, Γ_2 and Γ_3, such that $meas(\Gamma_1)>0$ and $meas(\Gamma_2)>0$. Moreover, Γ_2 is closed (see Fig. 1). The index, that follows a comma, represents the partial derivative with respect to the corresponding component of the spatial variable, e.g. $u_{i,j}=\partial u_i/\partial x_j$. We shall use the notation

$$\begin{aligned}
&V=\{\boldsymbol{v}=(v_i)\in H^1(\Omega)^d|\boldsymbol{v}=\boldsymbol{0}\text{ on }\Gamma_1\},\\
&Q=\{\boldsymbol{\tau}=(\tau_{ij})\in L^2(\Omega)^{d\times d}|\tau_{ij}=\tau_{ji}\},\\
&\mathbb{Y}=L^2(\Gamma_2)^d.
\end{aligned}$$

We assume that $\mathbb{Y}_{ad}$ is a closed convex subset of $\mathbb{Y}$. The spaces V and Q are real Hilbert spaces endowed with the inner products

$$(\boldsymbol{u},\boldsymbol{v})_V=\int_\Omega \boldsymbol{\varepsilon}(\boldsymbol{u})\cdot\boldsymbol{\varepsilon}(\boldsymbol{v})\,\mathrm{dx},$$

and the associated norms $\|\cdot\|_V$ and $\|\cdot\|_Q$, respectively. The deformation operator $\boldsymbol{\varepsilon}$ is defined by

$$\boldsymbol{\varepsilon}(\boldsymbol{v})=(\varepsilon_{ij}(\boldsymbol{v})),\quad \varepsilon_{ij}(\boldsymbol{v})=\frac{1}{2}(v_{i,j}+v_{j,i}),\quad \forall\boldsymbol{v}\in H^1(\Omega)^d.$$

Completeness of the space $(V,\|\cdot\|_V)$ follows with the assumption $meas(\Gamma_1)>0$, which allows the use of Korn's inequality.

For every element $\boldsymbol{v}\in V$, we still use $\boldsymbol{v}$ for the trace of $\boldsymbol{v}$ on the boundary Γ. In particular, v_ν and $\boldsymbol{v}_\tau$, the normal and the tangential component of $\boldsymbol{v}$ on Γ are given by $v_\nu=\boldsymbol{v}\cdot\boldsymbol{\nu}$, $\boldsymbol{v}_\tau=\boldsymbol{v}-v_\nu\boldsymbol{\nu}$, respectively. Similarly, for $\boldsymbol{\sigma}:\Omega\cup\Gamma\to\mathbb{S}^d$, we define its normal and the tangential components respectively by

$$\sigma_\nu=\boldsymbol{\sigma}\boldsymbol{\nu}\cdot\boldsymbol{\nu},\quad \boldsymbol{\sigma}_\tau=\boldsymbol{\sigma}\boldsymbol{\nu}-\sigma_\nu\boldsymbol{\nu}.$$

By the trace theorem of Sobolev spaces [1], there exists a positive constant c_0, depending only on Ω, Γ_1 and Γ_3, such that

$$\|\boldsymbol{v}\|_{L^2(\Gamma_3)^d}\le c_0\|\boldsymbol{v}\|_V,\qquad \forall\boldsymbol{v}\in V. \tag{2.1}$$

3 The model and variational formulation

Consider an elastic body such as shown in Fig. 1. The body is fixed on Γ_1 and therefore the displacement field vanishes there. We also assume that surface tractions of density $\boldsymbol{p}$ act on the Γ_2 (In examples, we only simulate the case that the tractions act on the top

https://doi.org/10.4208/cicp.120715.010216a Published online by Cambridge University Press

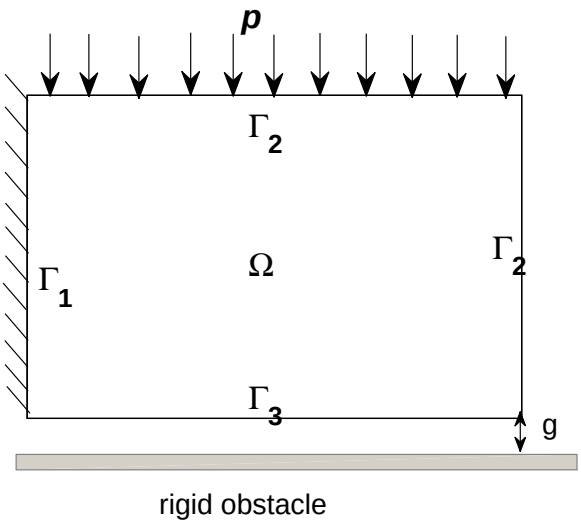


Figure 1: Physical setting model.

of the body, shown in Fig. 1). On Γ_3, the body may arrive in contact with a device, say an obstacle. We neglect the inertial term in the equation of motion and obtain the equilibrium of the process. The classical elastic problem with Signorini condition is:

Problem $\mathcal{P}_M$

Find a displacement $\boldsymbol{u}:\Omega\to\mathbb{R}^d$ *and a stress field* $\boldsymbol{\sigma}:\Omega\to\mathbb{S}^d$ *such that,*

$$\boldsymbol{\sigma}=\mathcal{A}\boldsymbol{\varepsilon}(\boldsymbol{u}) \qquad \text{in } \Omega, \tag{3.1}$$

$$-\mathrm{Div}\,\boldsymbol{\sigma}=\boldsymbol{f}_0 \qquad \text{in } \Omega, \tag{3.2}$$

$$\boldsymbol{u}=\boldsymbol{0} \qquad \text{on } \Gamma_1, \tag{3.3}$$

$$\boldsymbol{\sigma}\boldsymbol{\nu}=\boldsymbol{p} \qquad \text{on } \Gamma_2, \tag{3.4}$$

$$\left.\begin{array}{l}\sigma_\nu\le 0, u_\nu-g\le 0\\ \sigma_\nu(u_\nu-g)=0\\ \boldsymbol{\sigma}_\tau=\boldsymbol{0}\end{array}\right\} \qquad \text{on } \Gamma_3, \tag{3.5}$$

where $\boldsymbol{\varepsilon}(\boldsymbol{u})$ *is the linearized strain tensor.*

In Signorini condition (3.5), $g=g(\boldsymbol{x})\ge 0$ ($\boldsymbol{x}\in\Gamma_3$) is a gap between the boundary Γ_3 and obstacle. We assume that:

- Conditions of $\mathcal{A}$: the elasticity operator $\mathcal{A}:\Omega\times\mathbb{S}^d\to\mathbb{S}^d$ is a bounded fourth order

https://doi.org/10.4208/cicp.120715.010216a Published online by Cambridge University Press

tensor and symmetric positive definite, i.e.,

$$\begin{cases} \text{(a) } \mathcal{A}_{ijkl} \in L_\infty(\Omega); \text{ there exists a constant } M \text{ such that} \\ \qquad \max_{1\le i,j,k,l\le d} \|\mathcal{A}_{ijkl}\| \le M. \\ \text{(b) } \mathcal{A}_{ijkl}(\boldsymbol{x}) = \mathcal{A}_{klij}(\boldsymbol{x}) = \mathcal{A}_{jikl}(\boldsymbol{x}) \text{ a.e. in } \Omega, 1\le i,j,k,l\le d. \\ \text{(c) There exists a constant } m>0 \text{ such that a.e. in } \Omega, \\ \qquad \mathcal{A}_{ijkl}(\boldsymbol{x})\boldsymbol{\varepsilon}_{ij}\boldsymbol{\varepsilon}_{kl} \ge m\, \boldsymbol{\varepsilon}_{ij}\boldsymbol{\varepsilon}_{ij}, \\ \qquad \text{for every } \boldsymbol{\varepsilon}\in\mathbb{R}^{d\times d} \text{ such that } \boldsymbol{\varepsilon}_{ij}=\boldsymbol{\varepsilon}_{ji}. \end{cases} \tag{3.6}$$

- Conditions of the body force $\boldsymbol{f}_0$ and surface traction $\boldsymbol{p}$:

$$\boldsymbol{f}_0 \in L^2(\Omega)^d, \quad \boldsymbol{p}\in\mathbb{Y}. \tag{3.7}$$

- Conditions of the gap g:

$$\begin{cases} \text{(a) } g:\Gamma_3\to[0,+\infty). \\ \text{(b) There exists } G>0 \text{ such that } g(\boldsymbol{x})\le G, \text{ a.e. } \boldsymbol{x}\in\Gamma_3. \\ \text{(c) The mapping } \boldsymbol{x}\mapsto g(\boldsymbol{x}) \text{ is continuous on } \Gamma_3. \end{cases} \tag{3.8}$$

For the weak formulation of the problem $\mathcal{P}_M$ (3.1)-(3.5), let us introduce the set of admissible displacements

$$U=\{\boldsymbol{v}\in V | v_\nu \le g \text{ a.e. on } \Gamma_3\}.$$

Obviously, it is a non-empty closed convex set of V and denoted by U_0 in the special case of $g=0$. By Signorini condition (3.5), we have

$$\int_{\Gamma_3}\boldsymbol{\sigma v}\cdot(\boldsymbol{v}-\boldsymbol{u})ds = \int_{\Gamma_3}\sigma_\nu(v_\nu-g)\,\mathrm{ds}\ge 0.$$

We also define

$$a(\boldsymbol{u},\boldsymbol{v}) = \int_\Omega \mathcal{A}\boldsymbol{\varepsilon}(\boldsymbol{u})\cdot\boldsymbol{\varepsilon}(\boldsymbol{v})\,\mathrm{dx}, \qquad \forall \boldsymbol{v}\in V, \tag{3.9}$$

$$(\boldsymbol{f},\boldsymbol{v}) = \int_\Omega \boldsymbol{f}_0\cdot\boldsymbol{v}\,\mathrm{dx}+\int_{\Gamma_2}\boldsymbol{p}\cdot\boldsymbol{v}\,\mathrm{ds}, \qquad \forall \boldsymbol{v}\in V, \tag{3.10}$$

where the bilinear form $a: H^1(\Omega)\times H^1(\Omega)\to\mathbb{R}$ and the function $\boldsymbol{f}\in V$. The variational form of the frictionless contact problem $\mathcal{P}_M$ is:

Problem $\mathcal{P}_V$:

Find a displacement $\boldsymbol{u}\in U$ *such that,*

$$a(\boldsymbol{u},\boldsymbol{v}-\boldsymbol{u})\ge(\boldsymbol{f},\boldsymbol{v}-\boldsymbol{u}), \quad \forall \boldsymbol{v}\in U. \tag{3.11}$$

For later use in error analysis of numerical approximations of this problem, we need a result on the uniform boundedness of the solution.

https://doi.org/10.4208/cicp.120715.010216a Published online by Cambridge University Press

Proposition 3.1. *Assume that the conditions* (3.6)-(3.8) *hold, then there exists a unique solution to the problem* $\mathcal{P}_V$. *Moreover, the solution satisfies*

$$\|\boldsymbol{u}\|_V \leq c_1\|\boldsymbol{f}\|_{V^*} + c_2 G, \tag{3.12}$$

where $\boldsymbol{f}$ *is defined as* (3.10) *and* G *is given in* (3.8).

Proof. For the existence and uniqueness of the solution of the problem $\mathcal{P}_V$, the proof is based on the results of elliptic variational inequalities and fixed point arguments [1, 22]. From conditions of $\mathcal{A}$, (3.8) and (3.9), we have

$$\begin{aligned} m\|\boldsymbol{u}\|_V^2 \leq a(\boldsymbol{u},\boldsymbol{u}) &= (\boldsymbol{f},\boldsymbol{v}) + (\sigma\boldsymbol{\nu},\boldsymbol{u})_{L^2(\Gamma_3)} \\ &= (\boldsymbol{f},\boldsymbol{v}) + (\sigma_\nu, g)_{L^2(\Gamma_3)} \\ &\leq C_1\|\boldsymbol{f}\|_{V^*}\|\boldsymbol{u}\|_V + C_2\|\sigma_\nu g\|_{L^2(\Gamma_3)} \\ &\leq C_1\|\boldsymbol{f}\|_{V^*}\|\boldsymbol{u}\|_V + C_2 M\|\boldsymbol{u}\|_V G. \end{aligned}$$

The proof is completed. □

4 Inverse problem

In this section, we consider the inverse problem to find $\boldsymbol{p}$ on Γ_2, such that

$$\boldsymbol{u}(\boldsymbol{p}) = \boldsymbol{u}_d \quad \text{in } \Omega, \tag{4.1}$$

where $\boldsymbol{u}$ is the solution of (3.1)-(3.5) and $\boldsymbol{u}_d$ is the observation data. Obviously, it is difficult to solve this problem. So firstly, let us introduce the set of admissible displacements

$$W = \{\boldsymbol{\xi} \in V | \boldsymbol{\xi}_\nu \leq g - \boldsymbol{u}_\nu \ \text{ a.e. on } \Gamma_3\}, \tag{4.2}$$

where $\boldsymbol{u}$ is the solution of the problem $\mathcal{P}_V$. Then the adjoint problem of the problem $\mathcal{P}_M$ is introduced:

Problem $\mathcal{P}_{DM}$:

Find a displacement $\boldsymbol{w} \in W$ *such that,*

$$\begin{aligned} &\overline{\sigma} = \mathcal{A}\varepsilon(\boldsymbol{w}) && \text{in } \Omega, \\ &\sigma = \mathcal{A}\varepsilon(\boldsymbol{u}(\boldsymbol{p})) && \text{in } \Omega, \\ &-\mathrm{Div}\,\overline{\sigma} = \boldsymbol{u}(\boldsymbol{p}) - \boldsymbol{u}_d && \text{in } \Omega, \\ &\boldsymbol{w} = \boldsymbol{0} && \text{on } \Gamma_1, \\ &\overline{\sigma}\boldsymbol{\nu} = \boldsymbol{0} && \text{on } \Gamma_2, \\ &\left.\begin{array}{l} \overline{\sigma_\nu} + \sigma_\nu \leq 0, w_\nu + u_\nu(\boldsymbol{p}) \leq g, \\ \overline{\sigma_\nu}(u_\nu(\boldsymbol{p}) - g) + \sigma_\nu w_\nu = 0, \overline{\sigma_\tau} = \boldsymbol{0} \end{array}\right\} && \text{on } \Gamma_3, \end{aligned} \tag{4.3}$$

https://doi.org/10.4208/cicp.120715.010216a Published online by Cambridge University Press

where $\boldsymbol{u}(\boldsymbol{p})$ is the solution of the problem $\mathcal{P}_M$ and its variational form as follows.

Problem $\mathcal{P}_{VD}$:

Find a displacement $\boldsymbol{w}\in W$ *such that,*

$$a(\boldsymbol{w},\boldsymbol{\xi}-\boldsymbol{w})\geq(\boldsymbol{u}(\boldsymbol{p})-\boldsymbol{u}_d,\boldsymbol{\xi}-\boldsymbol{w}),\qquad\forall\boldsymbol{\xi}\in W. \tag{4.4}$$

Since $\boldsymbol{u}_d$ and $\boldsymbol{u}(\boldsymbol{p})$ are given, by the Proposition 3.1, the problem $\mathcal{P}_{VD}$ has a unique solution. Lastly, we consider the following problem.

Problem IP_1:

Find a $\tilde{\boldsymbol{p}}\in\mathbb{Y}_{ad}$ *such that,*

$$I(\tilde{\boldsymbol{p}})=\inf_{\boldsymbol{p}\in\mathbb{Y}_{ad}}\frac{1}{2}\|\boldsymbol{u}(\boldsymbol{p})-\boldsymbol{u}_d\|_V^2, \tag{4.5}$$

where $\boldsymbol{u}(\boldsymbol{p})$ *is the solution of* $\mathcal{P}_V$.

We still denote by $\boldsymbol{p}$ the solution (or quasi-solution) of the problem IP_1 and by S the set of all quasi-solutions [23].

Theorem 4.1. *Assume that the conditions* (3.6)-(3.8) *hold, then the problem* IP_1 *has at least one solution.*

The proof of existence can be found in [3].

By Theorem 4.1, for any $\boldsymbol{p}\in S$, there exists at least one weak solution $\boldsymbol{u}(\boldsymbol{p})\in V$ of the problem $\mathcal{P}_V$. So we introduce a Tikhonov regularization to the problem IP_1.

Problem IP_2:

Find a $\boldsymbol{p}_\alpha\in\mathbb{Y}_{ad}$ *such that,*

$$J_\alpha(\boldsymbol{p}_\alpha)=\inf_{\boldsymbol{p}\in\mathbb{Y}_{ad}}J_\alpha(\boldsymbol{p}), \tag{4.6}$$

where

$$J_\alpha(\boldsymbol{p})=\frac{1}{2}\|\boldsymbol{u}(\boldsymbol{p})-\boldsymbol{u}_d\|_V^2+\frac{\alpha}{2}\|\boldsymbol{p}\|_{\mathbb{Y}}^2,$$

and $\boldsymbol{u}_d$ *is the observation data.*

Since

$$\begin{aligned}&J'_\alpha(\boldsymbol{p})\boldsymbol{q}=(\boldsymbol{u}(\boldsymbol{p})-\boldsymbol{u}_d,\boldsymbol{u}(\boldsymbol{q})-\boldsymbol{u}(\boldsymbol{0}))_V+\alpha(\boldsymbol{p},\boldsymbol{q})_{\mathbb{Y}},\\&J''_\alpha(\boldsymbol{p})\boldsymbol{q}^2=\|\boldsymbol{u}(\boldsymbol{q})-\boldsymbol{u}(\boldsymbol{0})\|_V^2+\alpha\|\boldsymbol{q}\|_{\mathbb{Y}}^2,\end{aligned} \tag{4.7}$$

for any $\alpha>0$ and $\boldsymbol{q}\neq0$, $J_\alpha(\cdot)$ is the strictly convex. Then, we show a well-posedness result and the first optimality condition of the solution:

https://doi.org/10.4208/cicp.120715.010216a Published online by Cambridge University Press

Proposition 4.1. *For any $\alpha>0$, the problem IP_2 has a unique solution $\boldsymbol{p}_\alpha\in\mathbb{Y}_{ad}$, which depends continuously on $\boldsymbol{f}_0$ and g. Moreover, $\boldsymbol{p}_\alpha$ is characterized by the inequality*

$$(\boldsymbol{w}(\boldsymbol{p}_\alpha)+\alpha\boldsymbol{p}_\alpha,\boldsymbol{q}-\boldsymbol{p}_\alpha)_{\mathbb{Y}}\geq 0, \tag{4.8}$$

where $\boldsymbol{q}\in\mathbb{Y}_{ad}$ has the same equilibrium state as $\boldsymbol{p}_\alpha$ and $\boldsymbol{w}(\boldsymbol{p}_\alpha)$ is the unique weak solution of the problem $\mathcal{P}_{VD}$.

Proof. Since $\mathbb{Y}_{ad}$ is a closed and convex set in the Hilbert space $\mathbb{Y}$, $J_\alpha(\cdot)$ is strictly convex over $\mathbb{Y}_{ad}$. By a standard result on convex minimization problems, a unique stable solution $\boldsymbol{p}_\alpha\in\mathbb{Y}_{ad}$ can be shown for the problem IP_2 [1,7]. Moreover, the solution satisfies the first order optimality condition

$$J'_\alpha(\boldsymbol{p}_\alpha)(\boldsymbol{q}-\boldsymbol{p}_\alpha)\geq 0,$$

where $\boldsymbol{q}\in\mathbb{Y}_{ad}$. Now we present the proof of the inequality (4.8). Let $\boldsymbol{p}_\alpha$, $\boldsymbol{q}\in\mathbb{Y}_{ad}$. From problem (4.4), we obtain

$$\int_\Omega \mathcal{A}\boldsymbol{\varepsilon}(\boldsymbol{w}(\boldsymbol{p}_\alpha))\cdot\boldsymbol{\varepsilon}(\boldsymbol{v})\,\mathrm{dx}=\int_\Omega(\boldsymbol{u}(\boldsymbol{p}_\alpha)-\boldsymbol{u}_d)\cdot\boldsymbol{v}\,\mathrm{dx}+\int_{\Gamma_3}\overline{\boldsymbol{\sigma}}\boldsymbol{\nu}\cdot\boldsymbol{v}\,\mathrm{ds}. \tag{4.9}$$

Let $\boldsymbol{u}(\boldsymbol{0})\in V$ be the weak solution of the problem $\mathcal{P}_V$ with replaced $\boldsymbol{p}$ by $\boldsymbol{0}$. The weak form of the problem $\mathcal{P}_M$ is

$$\int_\Omega \mathcal{A}\boldsymbol{\varepsilon}(\boldsymbol{u}(\boldsymbol{q})-\boldsymbol{u}(\boldsymbol{0}))\cdot\boldsymbol{\varepsilon}(\boldsymbol{v})\,\mathrm{dx}=\int_{\Gamma_3}(\boldsymbol{\sigma}(\boldsymbol{u}(\boldsymbol{q}))-\boldsymbol{\sigma}(\boldsymbol{u}(\boldsymbol{0})))\boldsymbol{\nu}\cdot\boldsymbol{v}\,\mathrm{ds}+\int_{\Gamma_2}\boldsymbol{q}\cdot\boldsymbol{v}\,\mathrm{ds}. \tag{4.10}$$

Takeing $\boldsymbol{v}=\boldsymbol{u}(\boldsymbol{q})-\boldsymbol{u}(\boldsymbol{0})$ in (4.9) and $\boldsymbol{v}=\boldsymbol{w}(\boldsymbol{p}_\alpha)$ in (4.10) and subtracting them, we deduce

$$\begin{aligned}\int_\Omega(\boldsymbol{u}(\boldsymbol{p}_\alpha)-\boldsymbol{u}_d)\cdot(\boldsymbol{u}(\boldsymbol{q})-\boldsymbol{u}(\boldsymbol{0}))\,\mathrm{dx}=&\int_{\Gamma_3}(\boldsymbol{\sigma}(\boldsymbol{u}(\boldsymbol{q}))-\boldsymbol{\sigma}(\boldsymbol{u}(\boldsymbol{0}))\boldsymbol{\nu}\cdot\boldsymbol{w}(\boldsymbol{p}_\alpha)\,\mathrm{ds}\\&+\int_{\Gamma_2}\boldsymbol{q}\cdot\boldsymbol{w}(\boldsymbol{p}_\alpha)\,\mathrm{ds}-\int_{\Gamma_3}\overline{\boldsymbol{\sigma}}\boldsymbol{\nu}\cdot(\boldsymbol{u}(\boldsymbol{q})-\boldsymbol{u}(\boldsymbol{0}))\,\mathrm{ds}.\end{aligned}$$

So, by the equality (4.7), we have

$$\begin{aligned}J'_\alpha(\boldsymbol{p}_\alpha)\boldsymbol{q}=&\int_{\Gamma_3}(\boldsymbol{\sigma}(\boldsymbol{u}(\boldsymbol{q}))-\boldsymbol{\sigma}(\boldsymbol{u}(\boldsymbol{0})))\boldsymbol{\nu}\cdot\boldsymbol{w}(\boldsymbol{p}_\alpha)\,\mathrm{ds}+(\boldsymbol{w}(\boldsymbol{p}_\alpha),\boldsymbol{q})_{\mathbb{Y}}\\&-\int_{\Gamma_3}\overline{\boldsymbol{\sigma}}\boldsymbol{\nu}\cdot(\boldsymbol{u}(\boldsymbol{q})-\boldsymbol{u}(\boldsymbol{0}))\,\mathrm{ds}+(\alpha\boldsymbol{p}_\alpha,\boldsymbol{q})_{\mathbb{Y}}.\end{aligned}$$

Hence,

$$\begin{aligned}J'_\alpha(\boldsymbol{p}_\alpha)\boldsymbol{q}-J'_\alpha(\boldsymbol{p}_\alpha)\boldsymbol{p}_\alpha=&(\boldsymbol{w}(\boldsymbol{p}_\alpha)+\alpha\boldsymbol{p}_\alpha,\boldsymbol{q})_{\mathbb{Y}}+(\sigma_\nu(\boldsymbol{u}(\boldsymbol{q}))-\sigma_\nu(\boldsymbol{u}(\boldsymbol{p}_\alpha)),w_\nu(\boldsymbol{p}_\alpha))_{L^2(\Gamma_3)}\\&-(\boldsymbol{w}(\boldsymbol{p}_\alpha)+\alpha\boldsymbol{p}_\alpha,\boldsymbol{p}_\alpha)_{\mathbb{Y}}-(\overline{\sigma_\nu},u_\nu(\boldsymbol{q})-u_\nu(\boldsymbol{p}_\alpha))_{L^2(\Gamma_3)}.\end{aligned}$$

There are two cases:

https://doi.org/10.4208/cicp.120715.010216a Published online by Cambridge University Press

(1) The body contacts with the foundation.

On Γ_3, the solution $\boldsymbol{u}$ of problem (3.1)-(3.5) and the solution $\boldsymbol{w}$ of its adjoint problem satisfy:

$$\begin{cases} \sigma_\nu \leq 0,\ u_\nu = g,\ \boldsymbol{\sigma}_\tau = \mathbf{0}, \\ w_\nu \leq 0,\ \sigma_\nu w_\nu = 0,\ \overline{\boldsymbol{\sigma}_\tau} = \mathbf{0}, \end{cases} \quad \text{on } \Gamma_3.$$

(2) The body does not contact with the foundation.

We get

$$\begin{cases} \sigma_\nu = 0, u_\nu \leq g,\ \boldsymbol{\sigma}_\tau = \mathbf{0} \\ \overline{\sigma_\nu} \leq 0, \overline{\sigma_\nu}(u_\nu - g) = 0,\ \overline{\boldsymbol{\sigma}_\tau} = \mathbf{0} \end{cases} \quad \text{on } \Gamma_3.$$

Keeping in mind of the assumption of $\boldsymbol{q}$, and by the case (1), we have

$$\begin{cases} (\sigma_\nu(\boldsymbol{u}(\boldsymbol{q})) - \sigma_\nu(\boldsymbol{u}(\boldsymbol{p}_\alpha)), w_\nu(\boldsymbol{p}_\alpha))_{L^2(\Gamma_3)} = 0, \\ (\sigma_\nu(\boldsymbol{w}(\boldsymbol{p}_\alpha)), u_\nu(\boldsymbol{q}) - u_\nu(\boldsymbol{p}_\alpha))_{L^2(\Gamma_3)} = 0, \end{cases} \quad \text{on } \Gamma_3,$$

and by the case (2),

$$\begin{cases} (\sigma_\nu(\boldsymbol{u}(\boldsymbol{q})) - \sigma_\nu(\boldsymbol{u}(\boldsymbol{p}_\alpha)), w_\nu(\boldsymbol{p}_\alpha))_{L^2(\Gamma_3)} = 0, \\ (\sigma_\nu(\boldsymbol{w}(\boldsymbol{p}_\alpha)), u_\nu(\boldsymbol{q}) - u_\nu(\boldsymbol{p}_\alpha))_{L^2(\Gamma_3)} \geq 0, \end{cases} \quad \text{on } \Gamma_3.$$

For both cases,

$$(\sigma_\nu(\boldsymbol{u}(\boldsymbol{q})) - \sigma_\nu(\boldsymbol{u}(\boldsymbol{p}_\alpha)), w_\nu(\boldsymbol{p}_\alpha))_{L^2(\Gamma_3)} - (\sigma_\nu(\boldsymbol{w}(\boldsymbol{p}_\alpha)), u_\nu(\boldsymbol{q}) - u_\nu(\boldsymbol{p}_\alpha))_{L^2(\Gamma_3)} \leq 0.$$

Thus, by the inequality $J'_\alpha(\boldsymbol{p}_\alpha)\boldsymbol{q} \geq J'_\alpha(\boldsymbol{p}_\alpha)\boldsymbol{p}_\alpha$, the inequality (4.8) follows. □

Because the problem IP_1 has at least one solution (Theorem 4.1), we have $S \neq \varnothing$. Moreover, it is straightforward to show that S is closed and convex. Denote by $\boldsymbol{p}^* \in S$ the unique function, such that

$$\|\boldsymbol{p}^*\|_{\mathbb{Y}} = \inf_{\boldsymbol{p} \in S} \|\boldsymbol{p}\|_{\mathbb{Y}}.$$

We have the results about $\boldsymbol{p}_\alpha$ as $\alpha \to 0^+$.

Proposition 4.2. *$\boldsymbol{p}_\alpha \to \boldsymbol{p}^* \in \mathbb{Y}$, as $\alpha \to 0^+$.*

Proof. Let $\boldsymbol{u}(\boldsymbol{p}^*)$ be the weak solution of problem (3.1)-(3.5) with $\boldsymbol{p}^* \in S$. Then from the equality (4.6),

$$\begin{aligned} J_\alpha(\boldsymbol{p}_\alpha) &= \frac{1}{2}\|\boldsymbol{u}(\boldsymbol{p}_\alpha) - \boldsymbol{u}_d\|_V^2 + \frac{\alpha}{2}\|\boldsymbol{p}_\alpha\|_{\mathbb{Y}}^2 \\ &\leq J_\alpha(\boldsymbol{p}^*) = \frac{1}{2}\|\boldsymbol{u}(\boldsymbol{p}^*) - \boldsymbol{u}_d\|_V^2 + \frac{\alpha}{2}\|\boldsymbol{p}^*\|_{\mathbb{Y}}^2. \end{aligned}$$

https://doi.org/10.4208/cicp.120715.010216a Published online by Cambridge University Press

And from (4.5), we know

$$\frac{1}{2}\|\boldsymbol{u}(\boldsymbol{p}_\alpha)-\boldsymbol{u}_d\|_V^2 \geq \frac{1}{2}\|\boldsymbol{u}(\boldsymbol{p}^*)-\boldsymbol{u}_d\|_V^2.$$

Hence, we have $\|\boldsymbol{p}_\alpha\|_{\mathbb{Y}} \leq \|\boldsymbol{p}^*\|_{\mathbb{Y}}$. Since $\boldsymbol{u}(\boldsymbol{p}_\alpha)$ is the weak solution of the problem $\mathcal{P}_V$ with $\boldsymbol{p}$ replaced by $\boldsymbol{p}_\alpha$. Then from the estimate inequality (3.12), we obtain

$$\begin{aligned}\|\boldsymbol{u}(\boldsymbol{p}_\alpha)\|_V &\leq c_1(\|\boldsymbol{f}_0\|_V+\|\boldsymbol{p}_\alpha\|_{\mathbb{Y}})+c_2\|g\|_{L^2(\Gamma_3)}\\ &\leq c_1(\|\boldsymbol{f}_0\|_V+\|\boldsymbol{p}^*\|_{\mathbb{Y}})+c_2G.\end{aligned}$$

Similarly, let $\boldsymbol{w}(\boldsymbol{p}_\alpha)\in V$ be the unique weak solution of corresponding adjoint problem. Then, with the proof of the Proposition 3.1, we have

$$\|\boldsymbol{w}(\boldsymbol{p}_\alpha)\|_V \leq c_3\|\boldsymbol{u}(\boldsymbol{p}_\alpha)-\boldsymbol{u}_d\|_V+c_4.$$

Thus, $\boldsymbol{p}_\alpha$, $\boldsymbol{u}(\boldsymbol{p}_\alpha)$ and $\boldsymbol{w}(\boldsymbol{p}_\alpha)$ are uniformly bounded w.r.t.α in the spaces $\mathbb{Y}$ and V respectively. Therefore, there are some elements $\boldsymbol{p}_0\in\mathbb{Y}$, $\boldsymbol{u}(\boldsymbol{p}_0)$, $\boldsymbol{w}(\boldsymbol{p}_0)\in V$, and a subsequence $\{\alpha'\}$ of α, as $\alpha'\to 0^+$, we have the following convergence relations:

$$\begin{aligned}&\boldsymbol{p}_{\alpha'} \rightharpoonup \boldsymbol{p}_0 && \text{in } \mathbb{Y},\\ &\boldsymbol{u}(\boldsymbol{p}_{\alpha'}) \rightharpoonup \boldsymbol{u}(\boldsymbol{p}_0) && \text{in } V,\\ &\boldsymbol{w}(\boldsymbol{p}_{\alpha'}) \rightharpoonup \boldsymbol{w}(\boldsymbol{p}_0) && \text{in } V.\end{aligned}$$

Using these convergence relations, and replacing α by α' in inequality (4.8) and let $\alpha'\to 0^+$, we get

$$(\boldsymbol{w}(\boldsymbol{p}_0),\boldsymbol{q}-\boldsymbol{p}_0)_{\mathbb{Y}}\geq 0.$$

This imply that $\boldsymbol{p}_0$ is a solution of the problem IP_2 with $\alpha=0$, and of course, a solution of the problem IP_1. So $\boldsymbol{p}_0\in S$ and

$$\liminf_{\alpha'\to 0^+}\|\boldsymbol{p}_{\alpha'}\|_{\mathbb{Y}} \leq \|\boldsymbol{p}^*\|_{\mathbb{Y}} \leq \|\boldsymbol{p}_0\|_{\mathbb{Y}}.$$

Thus, we obtain $\boldsymbol{p}_0=\boldsymbol{p}^*$. Since the limit $\boldsymbol{p}_0$ is unique, the entire family $\boldsymbol{p}_\alpha$ converges weakly to $\boldsymbol{p}^*$ in $\mathbb{Y}$ as $\alpha\to 0^+$. As a results, as $\alpha\to 0^+$, we have

$$\begin{aligned}\|\boldsymbol{p}_\alpha-\boldsymbol{p}^*\|_{\mathbb{Y}}^2 &= \|\boldsymbol{p}_\alpha\|_{\mathbb{Y}}^2-2(\boldsymbol{p}_{\alpha'},\boldsymbol{p}^*)_{\mathbb{Y}}+\|\boldsymbol{p}^*\|_{\mathbb{Y}}^2\\ &\leq 2\|\boldsymbol{p}^*\|_{\mathbb{Y}}^2-2(\boldsymbol{p}_{\alpha'},\boldsymbol{p}^*)_{\mathbb{Y}} \quad\to\quad 0,\end{aligned}$$

which shows the strong convergence of $\boldsymbol{p}_\alpha$ to $\boldsymbol{p}^*$ in $\mathbb{Y}$ as $\alpha\to 0^+$. □

https://doi.org/10.4208/cicp.120715.010216a Published online by Cambridge University Press

5 Numerical analysis

In order to write the discrete problem, we assume that Ω is a polygon and introduce a regular family $\{\mathcal{T}_h\}$ of triangulations of $\overline{\Omega}$ by (closed) triangles. The boundary of $\overline{\Omega}$ contains three parts, i.e., $\Gamma=\Gamma_1\cup\Gamma_2\cup\bigcup_{i=1}^{i_0}\Gamma_{3,i}$. Let $V_h\subset V$ be the corresponding finite element spaces of linear elements and $U^h=V_h\cap U$, $U_0^h=V_h\cap U_0$, $W^h=V_h\cap W$ be the finite element subset of U, U_0 and W respectively. An element from U^h and W^h are a continuous piecewise linear function with vanishing values at the finite element nodes lying on Γ_1, such that its normal component at any node on Γ_3 is non-positive.

The discrete formulation of the problem $\mathcal{P}_V$ and the problem $\mathcal{P}_{VD}$ are as follows.

Problem $\mathcal{P}_V^h$:

Find a displacement $\boldsymbol{u}^h\in U^h$ *such that,*

$$a(\boldsymbol{u}^h,\boldsymbol{v}^h-\boldsymbol{u}^h)\geq(\boldsymbol{f},\boldsymbol{v}^h-\boldsymbol{u}^h),\qquad\forall\boldsymbol{v}^h\in U^h. \tag{5.1}$$

Problem $\mathcal{P}_{VD}^h$:

Find a displacement $\boldsymbol{w}^h\in W^h$ *such that,*

$$a(\boldsymbol{w}^h,\boldsymbol{\xi}^h-\boldsymbol{w}^h)\geq(\boldsymbol{u}(\boldsymbol{p})-\boldsymbol{u}_d,\boldsymbol{\xi}^h-\boldsymbol{w}^h),\qquad\forall\boldsymbol{\xi}^h\in W^h. \tag{5.2}$$

With the assumptions of the data, the discrete variational inequality (5.1) has a unique solution. We can derive the a priori finite element error estimates [1, 9]:

$$\|\boldsymbol{u}-\boldsymbol{u}^h\|_V^2\leq c\inf_{\boldsymbol{v}^h\in U^h}\left(\|\boldsymbol{u}-\boldsymbol{v}^h\|_V^2+\int_{\Gamma_3}\boldsymbol{\sigma\nu}\cdot(\boldsymbol{v}^h-\boldsymbol{u})\,\mathrm{ds}\right).$$

Since $\boldsymbol{u}\in U$ and

$$\inf_{\boldsymbol{v}^h\in U^h}\left|\int_{\Gamma_3}\sigma_\nu(v_\nu^h-u_\nu)\,\mathrm{ds}\right|\leq h^2\|\sigma_\nu\|_{L^2(\Gamma_3)}\|\boldsymbol{u}\|_V. \tag{5.3}$$

We can obtain

$$\|\boldsymbol{u}-\boldsymbol{u}^h\|_V\leq ch(\|\boldsymbol{f}_0\|_V+\|\boldsymbol{p}\|_{\mathbb{Y}}+G).$$

Similarly, we define a discrete regularized objective functional:

$$J_\alpha^h(\boldsymbol{p})=\frac{1}{2}\|\boldsymbol{u}^h(\boldsymbol{p})-\boldsymbol{u}_d\|_V^2+\frac{\alpha}{2}\|\boldsymbol{p}\|_{\mathbb{Y}}^2,\quad\boldsymbol{p}\in\mathbb{Y}_{ad}.$$

It can also be verified that $J_\alpha^h(\cdot)$ is strictly convex, for $\alpha>0$.

For the surface tractions $\boldsymbol{p}$, we use piecewise constants to approximate it. We define

$$\mathbb{Y}^h=\{\boldsymbol{p}\in\mathbb{Y}\mid\boldsymbol{p}\text{ is constant in }\partial T\cap\Gamma_2,T\in\mathcal{T}_h\},$$

https://doi.org/10.4208/cicp.120715.010216a Published online by Cambridge University Press

and the orthogonal projection operator $\Pi^h:\mathbb{Y}\to\mathbb{Y}^h$ by

$$(\Pi^h\boldsymbol{p},\boldsymbol{q}^h)_{\mathbb{Y}}=(\boldsymbol{p},\boldsymbol{q}^h)_{\mathbb{Y}},\quad \forall\boldsymbol{p}\in\mathbb{Y},\ \boldsymbol{q}^h\in\mathbb{Y}^h. \tag{5.4}$$

Then we have the boundedness inequality

$$\|\Pi^h\boldsymbol{q}\|_{\mathbb{Y}}\le\|\boldsymbol{q}\|_{\mathbb{Y}},\quad \forall\boldsymbol{q}\in\mathbb{Y}, \tag{5.5}$$

and the error bound

$$\|\boldsymbol{q}-\Pi^h\boldsymbol{q}\|_{\mathbb{Y}}\le ch|\boldsymbol{q}|_{H^1(\Gamma_2)},\quad \forall\boldsymbol{q}\in H^1(\Gamma_2). \tag{5.6}$$

Set $\mathbb{Y}^h_{ad}=\mathbb{Y}^h\cap\mathbb{Y}_{ad}=\{\boldsymbol{p}\in\mathbb{Y}_{ad}\mid \boldsymbol{p}$ is constant in $\partial T\cap\Gamma_2, T\in\mathcal{T}_h\}$ and we introduce the following discrete optimization problem:

Problem IP_3:

Find a $\boldsymbol{p}^h_\alpha\in\mathbb{Y}^h_{ad}$ *such that,*

$$J^h_\alpha(\mathbf{p}^h_\alpha)=\inf_{\mathbf{p}^h\in\mathbb{Y}^h_{ad}}J^h_\alpha(\mathbf{p}^h). \tag{5.7}$$

Proposition 5.1. *For any* $\alpha>0$*, the problem* IP_3 *has a unique solution* $\boldsymbol{p}^h_\alpha\in\mathbb{Y}^h_{ad}$*, which depends continuously on* $\boldsymbol{f}_0$*,* g*. Moreover,* $\boldsymbol{p}^h_\alpha$ *is characterized by the inequality*

$$(\boldsymbol{w}^h(\boldsymbol{p}^h_\alpha)+\alpha\boldsymbol{p}^h_\alpha,\boldsymbol{q}^h-\boldsymbol{p}^h_\alpha)_{\mathbb{Y}}\ge 0, \tag{5.8}$$

where $\boldsymbol{q}^h\in\mathbb{Y}^h_{ad}$ *has the same equilibrium state as* $\boldsymbol{p}^h_\alpha$ *and* $\boldsymbol{w}^h(\boldsymbol{p}^h_\alpha)$ *is the unique weak solution of the problem* $\mathcal{P}^h_{VD}$*.*

Before deriving an error estimate for the finite element solution $\boldsymbol{p}^h_\alpha$ of the problem IP_3, we have the following error estimates.

Theorem 5.1. *For any* $\boldsymbol{p}^h\in\mathbb{Y}^h_{ad}$*, let* $\boldsymbol{w}$ *and* $\boldsymbol{w}^h$ *be the solutions of the problem* $\mathcal{P}_{VD}$ *and the problem* $\mathcal{P}^h_{VD}$*. Then*

$$\|\boldsymbol{w}-\boldsymbol{w}^h\|_V\le ch(\|\boldsymbol{f}_0\|_V+\|\boldsymbol{p}^h\|_{\mathbb{Y}}+G), \tag{5.9}$$

where G *is defined as* (3.8)*.*

Proof. Firstly, taking $\boldsymbol{v}=\boldsymbol{v}^h$ in problem (4.4), we have

$$\int_\Omega\mathcal{A}\boldsymbol{\varepsilon}(\boldsymbol{w})\cdot\boldsymbol{\varepsilon}(\boldsymbol{v}^h)\,\mathrm{dx}=\int_\Omega(\boldsymbol{u}-\boldsymbol{u}_d)\cdot\boldsymbol{v}^h\,\mathrm{dx}+\int_{\Gamma_3}\boldsymbol{\sigma}(\boldsymbol{w})\boldsymbol{\nu}\cdot\boldsymbol{v}^h\,\mathrm{ds}.$$

It follows from problem (5.2) that

$$\int_\Omega\mathcal{A}\boldsymbol{\varepsilon}(\boldsymbol{w}^h)\cdot\boldsymbol{\varepsilon}(\boldsymbol{v}^h)\,\mathrm{dx}=\int_\Omega(\boldsymbol{u}^h-\boldsymbol{u}_d)\cdot\boldsymbol{v}^h\,\mathrm{dx}+\int_{\Gamma_3}\boldsymbol{\sigma}(\boldsymbol{w}^h)\boldsymbol{\nu}\cdot\boldsymbol{v}^h\,\mathrm{ds}.$$

https://doi.org/10.4208/cicp.120715.010216a Published online by Cambridge University Press

Then subtracting the above two equations and using $\boldsymbol{v}^h-\boldsymbol{w}^h$ instead of $\boldsymbol{v}^h$ yields

$$\begin{aligned}&\int_\Omega(\mathcal{A}\boldsymbol{\varepsilon}(\boldsymbol{w})-\mathcal{A}\boldsymbol{\varepsilon}(\boldsymbol{w}^h))\cdot(\boldsymbol{\varepsilon}(\boldsymbol{w})-\boldsymbol{\varepsilon}(\boldsymbol{w}^h))\mathrm{dx}\\&=\int_\Omega(\mathcal{A}\boldsymbol{\varepsilon}(\boldsymbol{w})-\mathcal{A}\boldsymbol{\varepsilon}(\boldsymbol{w}^h))\cdot(\boldsymbol{\varepsilon}(\boldsymbol{w})-\boldsymbol{\varepsilon}(\boldsymbol{v}^h))\mathrm{dx}\\&\quad+\int_\Omega(\boldsymbol{u}-\boldsymbol{u}^h)\cdot(\boldsymbol{v}^h-\boldsymbol{w}^h)\mathrm{dx}+\int_{\Gamma_3}(\sigma_\nu(\boldsymbol{w})-\sigma_\nu(\boldsymbol{w}^h))(v_\nu^h-w_\nu^h)\mathrm{ds}.\end{aligned}\tag{5.10}$$

Using the conditions of $\mathcal{A}$ and conditions (3.5), we derive

$$\begin{aligned}m\|\boldsymbol{w}-\boldsymbol{w}^h\|_V^2\le c\inf_{v^h\in W^h}\Big(&\|\boldsymbol{w}-\boldsymbol{w}^h\|_V\|\boldsymbol{w}-\boldsymbol{v}^h\|_V+\int_{\Gamma_3}\sigma_\nu(\boldsymbol{w})(v_\nu^h-w_\nu)\mathrm{ds}\\&+\|\boldsymbol{u}-\boldsymbol{u}^h\|_V(\|\boldsymbol{w}-\boldsymbol{v}^h\|_V+\|\boldsymbol{w}-\boldsymbol{w}^h\|_V)\Big).\end{aligned}\tag{5.11}$$

Applying the inequality $ab\le\frac{a^2}{4\epsilon}+\epsilon b^2$ and taking $c(\epsilon_1+\epsilon_2)<m$, the inequality (5.11) gives

$$\|\boldsymbol{w}-\boldsymbol{w}^h\|_V^2\le c_1\inf_{v^h\in W^h}\Big(\|\boldsymbol{w}-\boldsymbol{v}^h\|_V^2/4\epsilon_1+\|\boldsymbol{u}-\boldsymbol{u}^h\|_V^2/4\epsilon_2+\int_{\Gamma_3}\sigma_\nu(\boldsymbol{w})(v_\nu^h-w_\nu)\mathrm{ds}\Big).$$

Since $\boldsymbol{w}\in W$ and the estimate (5.3), inequality (5.9) follows. □

Let

$$E^h(\boldsymbol{p}_\alpha)=\|\boldsymbol{p}_\alpha-\Pi^h\boldsymbol{p}_\alpha\|_{\mathbb{Y}}=\inf_{\boldsymbol{q}^h\in\mathbb{Y}_{ad}^h}\|\boldsymbol{p}_\alpha-\boldsymbol{q}^h\|_{\mathbb{Y}}.$$

Since $E^h(\boldsymbol{p})$ is generally expected to be small, we give an error estimate for $\boldsymbol{p}_\alpha$ w.r.t. h as follows.

Theorem 5.2. *Let $\boldsymbol{p}_\alpha\in\mathbb{Y}_{ad}$ and $\boldsymbol{p}_\alpha^h\in\mathbb{Y}_{ad}^h$ be the solutions of the problem IP_2 and the problem IP_3, respectively. Then*

$$\|\boldsymbol{p}_\alpha-\boldsymbol{p}_\alpha^h\|_{\mathbb{Y}}\le c(\alpha^{-1}h+\alpha^{-1/2}h^{1/2}E^h(\boldsymbol{p}_\alpha)^{1/2}).\tag{5.12}$$

Proof. For the left-hand side of (5.12), we have

$$\|\boldsymbol{p}_\alpha-\boldsymbol{p}_\alpha^h\|_{\mathbb{Y}}\le\|\boldsymbol{p}_\alpha-\widetilde{\boldsymbol{p}}_\alpha^h\|_{\mathbb{Y}}+\|\widetilde{\boldsymbol{p}}_\alpha^h-\boldsymbol{p}_\alpha^h\|_{\mathbb{Y}},\tag{5.13}$$

where $\widetilde{\boldsymbol{p}}_\alpha^h\in\mathbb{Y}_{ad}^h$ is the unique solution of the problem IP_3 with $J_\alpha^h(\cdot)$ replaced by $J_\alpha(\cdot)$. Then

$$(\boldsymbol{w}(\widetilde{\boldsymbol{p}}_\alpha^h)+\alpha\widetilde{\boldsymbol{p}}_\alpha^h,\,\boldsymbol{q}^h-\widetilde{\boldsymbol{p}}_\alpha^h)_{\mathbb{Y}}\ge0,\tag{5.14}$$

where $\widetilde{\boldsymbol{u}}_\alpha^H=:\boldsymbol{u}(\widetilde{\boldsymbol{p}}_\alpha^h)$ is the weak solution of the problem $\mathcal{P}_V$ with $\boldsymbol{p}$ replaced by $\widetilde{\boldsymbol{p}}_\alpha^h$ and $\widetilde{\boldsymbol{w}}_\alpha^H=:\boldsymbol{w}(\widetilde{\boldsymbol{p}}_\alpha^h)$ is the solution of its adjoint problem.

https://doi.org/10.4208/cicp.120715.010216a Published online by Cambridge University Press

Only for simplicity, we take $\boldsymbol{u}_\alpha =: \boldsymbol{u}(\boldsymbol{p}_\alpha)$, $\boldsymbol{w}_\alpha =: \boldsymbol{w}(\boldsymbol{p}_\alpha)$. Substituting $\boldsymbol{q} = \widetilde{\boldsymbol{p}}_\alpha^h$ in (4.8) and $\boldsymbol{q}^h = \Pi^h \boldsymbol{p}_\alpha$ in (5.14), and adding the resulting inequalities, we get

$$\begin{aligned}\alpha\|\widetilde{\boldsymbol{p}}_\alpha^h - \boldsymbol{p}_\alpha\|_{\mathbb{Y}}^2 &= \alpha(\widetilde{\boldsymbol{p}}_\alpha^h - \boldsymbol{p}_\alpha, \widetilde{\boldsymbol{p}}_\alpha^h - \boldsymbol{p}_\alpha)_{\mathbb{Y}} \le \alpha(\widetilde{\boldsymbol{p}}_\alpha^h, \widetilde{\boldsymbol{p}}_\alpha^h - \boldsymbol{p}_\alpha)_{\mathbb{Y}} + (\boldsymbol{w}_\alpha, \widetilde{\boldsymbol{p}}_\alpha^h - \boldsymbol{p}_\alpha)_{\mathbb{Y}} \\ &\le \alpha(\widetilde{\boldsymbol{p}}_\alpha^h, \Pi^h \boldsymbol{p}_\alpha - \boldsymbol{p}_\alpha)_{\mathbb{Y}} + (\widetilde{\boldsymbol{w}}_\alpha^H, \Pi^h \boldsymbol{p}_\alpha - \widetilde{\boldsymbol{p}}_\alpha^h)_{\mathbb{Y}} + (\boldsymbol{w}_\alpha, \widetilde{\boldsymbol{p}}_\alpha^h - \boldsymbol{p}_\alpha)_{\mathbb{Y}} \\ &= (\widetilde{\boldsymbol{w}}_\alpha^H + \alpha\widetilde{\boldsymbol{p}}_\alpha^h, \Pi^h \boldsymbol{p}_\alpha - \boldsymbol{p}_\alpha)_{\mathbb{Y}} + (\boldsymbol{w}_\alpha - \widetilde{\boldsymbol{w}}_\alpha^H, \widetilde{\boldsymbol{p}}_\alpha^h - \boldsymbol{p}_\alpha)_{\mathbb{Y}}. \end{aligned} \tag{5.15}$$

It follows from the problem $\mathcal{P}_M$ and the problem $\mathcal{P}_{DM}$ that

$$\int_\Omega \mathcal{A}\boldsymbol{\varepsilon}(\boldsymbol{u}_\alpha)\cdot\boldsymbol{\varepsilon}(\boldsymbol{v})\,\mathrm{d}x = \int_\Omega \boldsymbol{f}_0\cdot\boldsymbol{v}\,\mathrm{d}x + \int_{\Gamma_2} \boldsymbol{p}_\alpha\cdot\boldsymbol{v}\,\mathrm{d}s + \int_{\Gamma_3} \sigma(\boldsymbol{u}_\alpha)\boldsymbol{\nu}\cdot\boldsymbol{v}\,\mathrm{d}s,$$

and

$$\int_\Omega \mathcal{A}\boldsymbol{\varepsilon}(\boldsymbol{w}_\alpha)\cdot\boldsymbol{\varepsilon}(\boldsymbol{v})\,\mathrm{d}x = \int_\Omega (\boldsymbol{u}_\alpha - \boldsymbol{u}_d)\cdot\boldsymbol{v}\,\mathrm{d}s + \int_{\Gamma_3} \sigma(\boldsymbol{w}_\alpha)\boldsymbol{\nu}\cdot\boldsymbol{v}\,\mathrm{d}s.$$

Thus,

$$\begin{aligned}\int_\Omega (\mathcal{A}\boldsymbol{\varepsilon}(\widetilde{\boldsymbol{u}}_\alpha^H) - \mathcal{A}\boldsymbol{\varepsilon}(\boldsymbol{u}_\alpha))\cdot\boldsymbol{\varepsilon}(\boldsymbol{v})\,\mathrm{d}x &= \int_{\Gamma_2} (\widetilde{\boldsymbol{p}}_\alpha^h - \boldsymbol{p}_\alpha)\cdot\boldsymbol{v}\,\mathrm{d}s \\ &\quad + \int_{\Gamma_3} (\sigma(\widetilde{\boldsymbol{u}}_\alpha^H) - \sigma(\boldsymbol{u}_\alpha))\boldsymbol{\nu}\cdot\boldsymbol{v}\,\mathrm{d}s, \end{aligned} \tag{5.16}$$

and

$$\begin{aligned}\int_\Omega (\mathcal{A}\boldsymbol{\varepsilon}(\boldsymbol{w}_\alpha) - \mathcal{A}\boldsymbol{\varepsilon}(\widetilde{\boldsymbol{w}}_\alpha^H))\cdot\boldsymbol{\varepsilon}(\boldsymbol{v})\,\mathrm{d}x &= \int_\Omega (\boldsymbol{u}_\alpha - \widetilde{\boldsymbol{u}}_\alpha^H)\cdot\boldsymbol{v}\,\mathrm{d}s \\ &\quad + \int_{\Gamma_3} (\sigma(\boldsymbol{w}_\alpha) - \sigma(\widetilde{\boldsymbol{w}}_\alpha^H))\boldsymbol{\nu}\cdot\boldsymbol{v}\,\mathrm{d}s. \end{aligned} \tag{5.17}$$

Applying conditions of $\mathcal{A}$, and replacing $\boldsymbol{v}$ with $\boldsymbol{w}_\alpha - \widetilde{\boldsymbol{w}}_\alpha^H$ in (5.16) and $\boldsymbol{v}$ with $\widetilde{\boldsymbol{u}}_\alpha^H - \boldsymbol{u}_\alpha$ in (5.17), we obtain

$$(\boldsymbol{w}_\alpha - \widetilde{\boldsymbol{w}}_\alpha^H, \widetilde{\boldsymbol{p}}_\alpha^h - \boldsymbol{p}_\alpha)_{\mathbb{Y}} = -\|\boldsymbol{u}_\alpha - \widetilde{\boldsymbol{u}}_\alpha^H\|_V^2. \tag{5.18}$$

For the first term on the right-hand side of (5.15), we have from (5.4), (5.6), (4.8) and $\widetilde{\boldsymbol{w}}_\alpha^H \in H^2(\Omega)$

$$\begin{aligned}&(\widetilde{\boldsymbol{w}}_\alpha^H + \alpha\widetilde{\boldsymbol{p}}_\alpha^h, \Pi^h \boldsymbol{p}_\alpha - \boldsymbol{p}_\alpha)_{\mathbb{Y}} \\ &= (\widetilde{\boldsymbol{w}}_\alpha^H - \Pi^h\widetilde{\boldsymbol{w}}_\alpha^H, \Pi^h \boldsymbol{p}_\alpha - \boldsymbol{p}_\alpha)_{\mathbb{Y}} + (\alpha\widetilde{\boldsymbol{p}}_\alpha^h + \Pi^h\widetilde{\boldsymbol{w}}_\alpha^H, \Pi^h \boldsymbol{p}_\alpha - \boldsymbol{p}_\alpha)_{\mathbb{Y}} \\ &\le chE^h(\boldsymbol{p}_\alpha) + \alpha(\Pi^h \boldsymbol{p}_\alpha - \widetilde{\boldsymbol{p}}_\alpha^h, \boldsymbol{p}_\alpha - \Pi^h \boldsymbol{p}_\alpha)_{\mathbb{Y}} \\ &= chE^h(\boldsymbol{p}_\alpha) + \alpha(\Pi^h \boldsymbol{p}_\alpha - \widetilde{\boldsymbol{p}}_\alpha^h, \boldsymbol{p}_\alpha)_{\mathbb{Y}} - \alpha(\Pi^h \boldsymbol{p}_\alpha - \widetilde{\boldsymbol{p}}_\alpha^h, \Pi^h \boldsymbol{p}_\alpha)_{\mathbb{Y}} \\ &= chE^h(\boldsymbol{p}_\alpha) + \alpha(\Pi^h \boldsymbol{p}_\alpha - \widetilde{\boldsymbol{p}}_\alpha^h, \boldsymbol{p}_\alpha)_{\mathbb{Y}} - \alpha(\Pi^h \boldsymbol{p}_\alpha - \widetilde{\boldsymbol{p}}_\alpha^h, \boldsymbol{p}_\alpha)_{\mathbb{Y}} \\ &= chE^h(\boldsymbol{p}_\alpha). \end{aligned} \tag{5.19}$$

https://doi.org/10.4208/cicp.120715.010216a Published online by Cambridge University Press

Therefore, from the above inequality, we obtain

$$\alpha\|\widetilde{\boldsymbol{p}}_\alpha^h-\boldsymbol{p}_\alpha\|_{\mathbb{Y}}^2\le chE^h(\boldsymbol{p}_\alpha)-\|\boldsymbol{u}_\alpha-\widetilde{\boldsymbol{u}}_\alpha^H\|_V^2,$$

which gives

$$\|\widetilde{\boldsymbol{p}}_\alpha^h-\boldsymbol{p}_\alpha\|_{\mathbb{Y}}\le c\alpha^{-1/2}h^{1/2}E^h(\boldsymbol{p}_\alpha)^{1/2}. \tag{5.20}$$

Similarly, replacing $\boldsymbol{q}^h$ with $\widetilde{\boldsymbol{p}}_\alpha^h$ in (5.8) and $\boldsymbol{q}^h$ with $\boldsymbol{p}_\alpha^h$ in (5.14), and adding the two inequalities, we get

$$\begin{aligned}\alpha\|\widetilde{\boldsymbol{p}}_\alpha^h-\boldsymbol{p}_\alpha^h\|_{\mathbb{Y}}^2&\le(\boldsymbol{w}(\widetilde{\boldsymbol{p}}_\alpha^h)-\boldsymbol{w}^h(\boldsymbol{p}_\alpha^h),\boldsymbol{p}_\alpha^h-\widetilde{\boldsymbol{p}}_\alpha^h)_{\mathbb{Y}}\\&=(\boldsymbol{w}(\widetilde{\boldsymbol{p}}_\alpha^h)-\boldsymbol{w}(\boldsymbol{p}_\alpha^h),\boldsymbol{p}_\alpha^h-\widetilde{\boldsymbol{p}}_\alpha^h)_{\mathbb{Y}}+(\boldsymbol{w}(\boldsymbol{p}_\alpha^h)-\boldsymbol{w}^h(\boldsymbol{p}_\alpha^h),\boldsymbol{p}_\alpha^h-\widetilde{\boldsymbol{p}}_\alpha^h)_{\mathbb{Y}}.\end{aligned}$$

From (5.9), we have

$$(\boldsymbol{w}(\boldsymbol{p}_\alpha^h)-\boldsymbol{w}^h(\boldsymbol{p}_\alpha^h),\boldsymbol{p}_\alpha^h-\widetilde{\boldsymbol{p}}_\alpha^h)_{\mathbb{Y}}\le ch\|\widetilde{\boldsymbol{p}}_\alpha^h-\boldsymbol{p}_\alpha^h\|_{\mathbb{Y}},$$

and

$$(\boldsymbol{w}(\widetilde{\boldsymbol{p}}_\alpha^h)-\boldsymbol{w}(\boldsymbol{p}_\alpha^h),\boldsymbol{p}_\alpha^h-\widetilde{\boldsymbol{p}}_\alpha^h)_{\mathbb{Y}}=-\|\boldsymbol{u}_\alpha-\widetilde{\boldsymbol{u}}_\alpha^H\|_V^2.$$

Hence,

$$\alpha\|\widetilde{\boldsymbol{p}}_\alpha^h-\boldsymbol{p}_\alpha^h\|_{\mathbb{Y}}\le ch. \tag{5.21}$$

So, by inequalities (5.13), (5.20) and (5.21), the error estimate (5.12) follows and the proof is completed. □

6 Numerical examples

In this section, several examples of inverse elastic problems are presented in two-dimensional case (See Fig. 1). Recalling the problem $\mathcal{P}_M$ in Section 3 and the problem IP_2 in Section 4, we propose an iterative optimization algorithm to reconstruct $\boldsymbol{p}$.

6.1 Iterative optimization algorithm

The iterative optimization algorithm (Algorithm 6.1) constructs three sequences $\{\boldsymbol{p}_\alpha^k\}$, $\{\boldsymbol{u}^k\}$ and $\{\boldsymbol{w}^k\}$. The initial guess $\boldsymbol{p}_\alpha^0$ can be chosen arbitrarily. With $\boldsymbol{p}_\alpha^{k-1}$, the solution $\{\boldsymbol{u}^k\}$ is obtained by solving the problem $\mathcal{P}_M$ and $\{\boldsymbol{w}^k\}$ is the solution of its adjoint problem. At k-th iteration, $\boldsymbol{p}_\alpha^k$ is updated by $J'_\alpha(\boldsymbol{p}_\alpha^{k-1})=0$ (i.e., the equality holds in (5.8)). Due to Theorem 5.2, the convergence of the algorithm depends on the regularization parameter α. Numerical results will illustrate the efficiency of the algorithm.

https://doi.org/10.4208/cicp.120715.010216a Published online by Cambridge University Press

Algorithm 6.1 Iterative optimization algorithm recovering $\boldsymbol{p}$

Require: $\boldsymbol{u}_d$ the observation data; $\epsilon>0$ the stop criterion;

1: **Initialization:** $\boldsymbol{p}_\alpha^0=\boldsymbol{0}$ and $k=1$.
2: **while** $\|\delta\boldsymbol{p}_\alpha^k\|>\epsilon$ **do**
3: Solve (5.1) with $\boldsymbol{p}_\alpha^{k-1}$, and get $\boldsymbol{u}^k$.
4: Solve (5.2) with $\boldsymbol{u}^h=\boldsymbol{u}^k$, and get $\boldsymbol{w}^k$.
5: Compute $\delta\boldsymbol{p}_\alpha^k=-\boldsymbol{w}^k/\alpha$, and update $\boldsymbol{p}_\alpha^k=\boldsymbol{p}_\alpha^{k-1}+\delta\boldsymbol{p}_\alpha^k$.
6: Set $k:=k+1$.
7: **end while**

6.2 Three examples

To show the efficiency of Algorithm 6.1, we give three different $\boldsymbol{p}$ in the following three examples respectively, and observe the recovery elastic bodies in the different equilibrium states with different noise levels. In all examples, we only focus on the case that the traction acts on $[0,L_1]\times\{L_2\}$, the top of the boundary. Of course, this could be easily extended to more general cases, e.g., the traction is not free on the whole Γ_2. It should be noted that this algorithm does not need any special requirements for the initial guess $\boldsymbol{p}_\alpha^0$. Moreover, $\boldsymbol{p}_\alpha^0$ is independent of the observation data $\boldsymbol{u}_d$. Therefore, for simplicity, all initial guesses of $\boldsymbol{p}$ are taken as $\boldsymbol{0}$. In each one of all examples coarse mesh (30×10) and refine mesh (60×20) are adopted. Other parameters and data are employed in all examples as follows.

The domain $\Omega=(0,L_1)\times(0,L_2)$, $L_1=3m, L_2=1.5m$.

The boundary $\Gamma=\bigcup_{i=1}^3\Gamma_i$,

$$\begin{cases}\Gamma_1=\{0\}\times[0,L_2], & \text{the left-hand side,}\\ \Gamma_2=\Gamma\backslash(\Gamma_1\cup\Gamma_3), & \text{the top and the right-hand side,}\\ \Gamma_3=[0,L_1]\times\{0\}, & \text{the bottom.}\end{cases}$$

The elasticity tensor $\mathcal{A}$ satisfies

$$(\mathcal{A}\tau)_{ij}=\frac{E\kappa}{1-\kappa^2}(\tau_{11}+\tau_{22})\delta_{ij}+\frac{E}{1+\kappa}\tau_{ij},\quad 1\le i,j\le 2,$$

where $E=1000N/m^2$ is the Young modulus, $\kappa=0.3$ is the Poisson ratio of the material and δ_{ij} denotes the Kronecker symbol.

The parameter in Signorini condition $g=0.3m$.

The stop criterion $\epsilon=1e-3$.

The body force $\boldsymbol{f}_0=\boldsymbol{0}$.

A measure of the error between the exact $\boldsymbol{p}$ and the numerical approximation $\boldsymbol{p}_\alpha^h$ is defined as

$$Err(\boldsymbol{p}_\alpha^h):=\frac{\|\boldsymbol{p}_\alpha^h-\boldsymbol{p}\|_{\mathbb{Y}}}{\|\boldsymbol{p}\|_{\mathbb{Y}}}. \tag{6.1}$$

https://doi.org/10.4208/cicp.120715.010216a Published online by Cambridge University Press

Example 6.1. The exact traction is

$$\mathbf{p}=\begin{cases}\mathbf{0}, & (0,\ L_1/2)\times\{L_2\},\\ (0,-50), & [L_1/2,\ L_1]\times\{L_2\},\\ \mathbf{0}, & \{L_1\}\times(0,\ L_2).\end{cases} \tag{6.2}$$

In this example, the boundary condition of the elastic model is Neumann condition. Actually, with $\boldsymbol{p}$ (6.2), the elastic body does not contact with the rigid obstacle (See the left sub-graph of Fig. 2). In Fig. 2, the domain of black color is the initial location of the elastic body. While red color domain is the location of the equilibrium state. The uniform triangular meshes in black color are utilized for finite element methods. The location difference of two colors at each mesh point is the displacement $\boldsymbol{u}(\boldsymbol{p})$. On Γ_1, the body is clamped and therefore the displacement vanishes there.

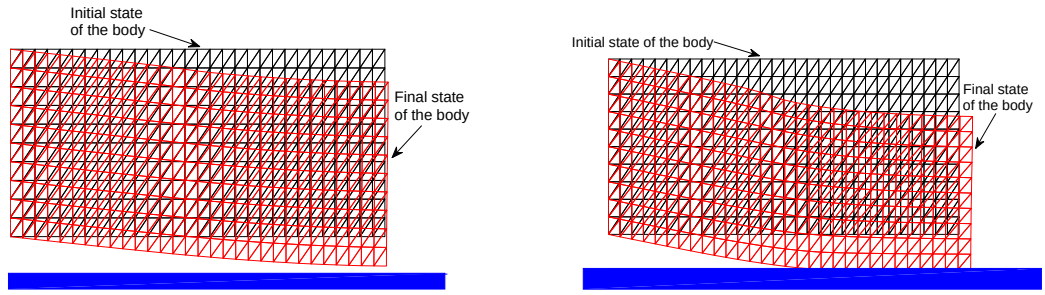


Figure 2: The elastic body in two different equilibrium stats: does not (the left sub-graph) and does (the right sub-graph) contact with rigid foundation. The domain of black color is the initial location of the elastic body. The red color domain is the location of the equilibrium state. The uniform triangular meshes in black color are utilized for finite element methods.

Fig. 3 shows numerical results based on the observation data $\boldsymbol{u}_d$ in the noise-free case. The blue solid line means the exact solution $\boldsymbol{p}$, while the red line with stars is the numerical solution $\boldsymbol{p}_\alpha^h$. The four different stages of solutions, that is, in the normal direction, in the tangential direction, on the boundary $[0,\ L_1]\times\{L_2\}$ and the boundary $\{L_1\}\times(0,\ L_2)$, are displayed in Fig. 3. It can be observed that numerical solution is very close to the exact solution. Although the tangential component in the left-top sub-graph has very small deflection near $x=3$ on the boundary $[0,\ L_1]\times\{L_2\}$, the normal component in the right-top sub-graph is well matched. Furthermore, on the boundary $[0,\ L_1]\times\{L_2\}$, both the tangential and the normal components of the exact solution are correctly recovered.

To compute more accurately and view more clearly the recovery solution, we uniformly refine the mesh. Each element of coarse mesh was divided by four, resulting $n_x=60$ in $(0,L_1)$ and $n_y=20$ in $(0,L_2)$. Numerical results in the fine mesh are displayed in Fig. 4.

In Table 1, we present the relative errors defined in (6.1) with different noise levels. Each row of Table 1 shows that the maximum error occurs in the last column (5% noise). This shows the fact that the sensitivity of the recovery solution to the noise level of the

https://doi.org/10.4208/cicp.120715.010216a Published online by Cambridge University Press

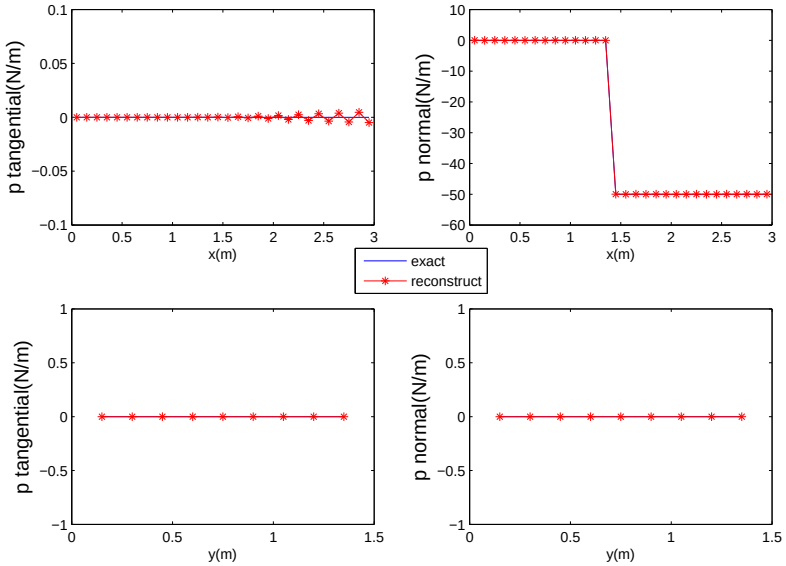


Figure 3: Numerical results based on the observation data $\boldsymbol{u}_d$ in the noise-free case. The mesh size is 30×10. The blue solid line means the exact solution $\mathbf{p}$ (6.2), while the red line with starts is the numerical solution $\mathbf{p}_\alpha^h$. Top row: on the boundary $[0,\ L_1]\times\{L_2\}$. Bottom row: on the boundary $\{L_1\}\times(0,\ L_2)$. Left column: in tangential direction. Right column: in normal direction.

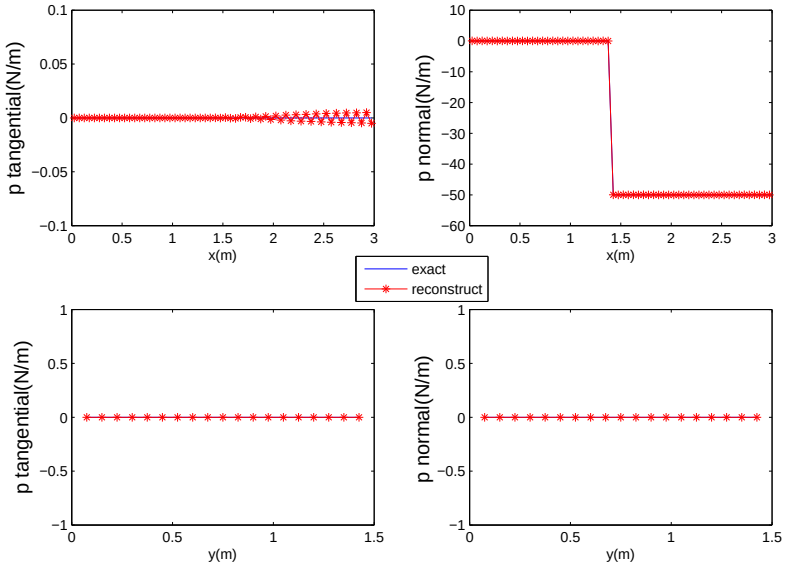


Figure 4: Numerical results based on the observation data $\boldsymbol{u}_d$ in the noise-free case. The mesh size is 60×20. The blue solid line means the exact solution $\mathbf{p}$ (6.2), while the red line with starts is the numerical solution $\mathbf{p}_\alpha^h$. Top row: on the boundary $[0,\ L_1]\times\{L_2\}$. Bottom row: on the boundary $\{L_1\}\times(0,\ L_2)$. Left column: in tangential direction. Right column: in normal direction.

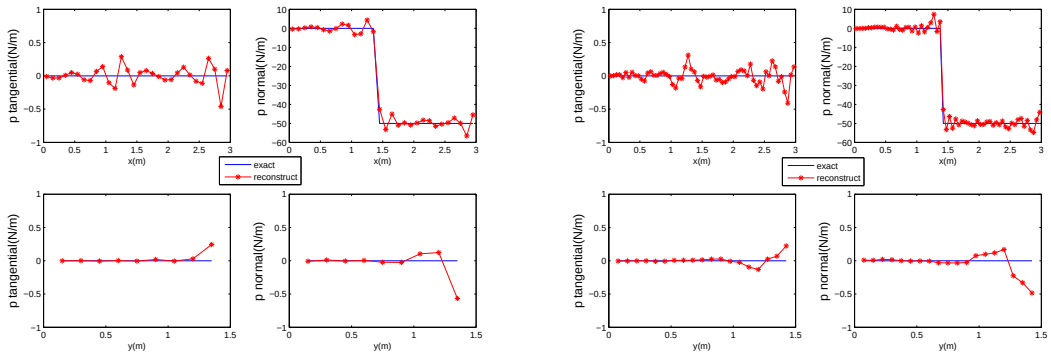
https://doi.org/10.4208/cicp.120715.010216a Published online by Cambridge University Press

Table 1: The error defined in (6.1) for Example 6.1.

α	mesh size	noise-free	2% noise	5% noise
1.0×10^{-5}	$n_x=30, n_y=10$	2.8144e-4	6.4349e-2	2.1166e-1
5.0×10^{-5}	$n_x=60, n_y=20$	1.8961e-4	6.1002e-2	1.4592e-1

observation data. Furthermore, the errors in the fine mesh is smaller than that in coarse mesh. Hence the mesh refinement can be applied to improve the accuracy of numerical solutions.

Fig. 5 depicts the numerical solution based on the observation data $\boldsymbol{u}_d$ with 2% noise. Compared with Fig. 3 and Fig. 4, here numerical solution obviously has oscillations. The bottom sub-graphs in part (a) of Fig. 5 shows that on the top side of the boundary $\{L_1\}\times(0,\ L_2)$, numerical solution deviates from the exact $\boldsymbol{p}$. Further, on the boundary $[0,\ L_1]\times\{L_2\}$, the oscillation becomes severe. From the left-top sub-graph in part (a) of Fig. 5, the maximum oscillation locates at nearly $x=2.85$. The second major oscillation locates at nearly $x=1.35$. Observing the right-top sub-graph in part (a) of Fig. 5, we can find evidently that the normal component of $\boldsymbol{p}$ is non-smooth at $x=1.4$ and discontinuous at $x=3$. Moreover, from numerical results in the refinement mesh displayed in part (b) of Fig. 5, we note the fact that the amplitudes of oscillations do not have evident change compared with that in coarse mesh. We may conclude that the oscillations, especial the first and the second major oscillations, come from the non-smoothness (including the discontinuousness) of $\boldsymbol{p}$.

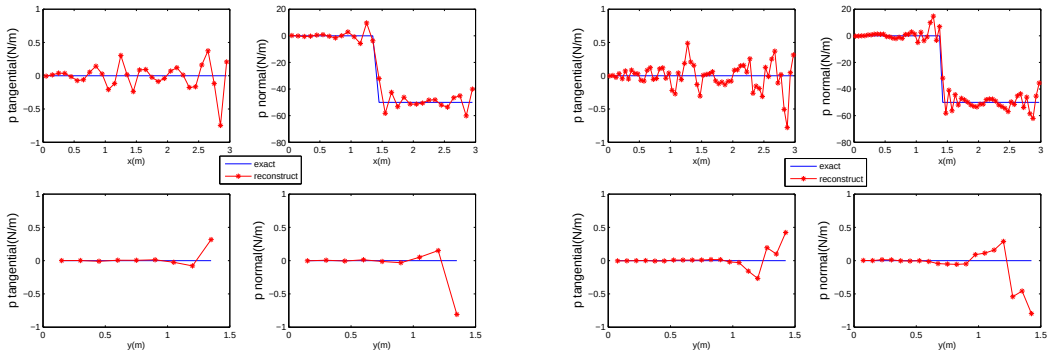


(a) 2% noise in coarse mesh (b) 2% noise in refinement mesh

Figure 5: Numerical results based on the observation data $\boldsymbol{u}_d$ with 2% noise. The blue solid line means the exact solution $\mathbf{p}$ (6.2), while the red line with starts is the numerical solution $\mathbf{p}_\alpha^h$. Top row: on the boundary $[0,\ L_1]\times\{L_2\}$. Bottom row: on the boundary $\{L_1\}\times(0,\ L_2)$. Left column: in tangential direction. Right column: in normal direction.

For the case of 5% noise, we show, in Fig. 6, numerical results in the coarse mesh and the fine mesh respectively for a comparison. It can be noted that the amplitudes

https://doi.org/10.4208/cicp.120715.010216a Published online by Cambridge University Press



(a) 5% noise in coarse mesh (b) 5% noise in refinement mesh

Figure 6: Numerical results based on the observation data $\boldsymbol{u}_d$ with 5% noise. The blue solid line means the exact solution $\mathbf{p}$ (6.2), while the red line with starts is the numerical solution $\mathbf{p}_\alpha^h$. Top row: on the boundary $[0,\ L_1]\times\{L_2\}$. Bottom row: on the boundary $\{L_1\}\times(0,\ L_2)$. Left column: in tangential direction. Right column: in normal direction.

of oscillations become larger than that in the case of 2% noise. The first and the second major oscillations of the tangential components still locate at nearly $x=1.35$ and $x=2.85$ respectively.

Example 6.2. The exact traction is

$$\mathbf{p}=\begin{cases}\mathbf{0}, & (0,\ L_1/2)\times\{L_2\},\\ (0,-150), & [L_1/2,\ L_1]\times\{L_2\},\\ \mathbf{0}, & \{L_1\}\times(0,\ L_2).\end{cases} \tag{6.3}$$

In this example, the absolute value of the vertical component of $\boldsymbol{p}$ (6.3) is bigger than that in Example 6.1. It is big enough to make the elastic body in equilibrium state contacting with the rigid obstacle Γ_3 (See the right sub-graph of Fig. 2). In Fig. 7, it shows the evolution of the error with respect to regularization parameter α^{-1} for the coarse mesh (30×10). As can be seen, the linear convergence of the algorithm is obtained (see Theorem 5.2). In Fig. 8 and Fig. 9, we show numerical results in the noise-free case with the coarse mesh and the fine mesh respectively. Similarly as Example 6.2, recovered numerical solutions are close to the exact solutions. In Table 2, we present the relative errors defined in (6.1) with different noise levels.

Table 2: The error defined in (6.1) for Example 6.2.

α	mesh size	noise-free	2% noise	5% noise
1.0×10^{-5}	$n_x=30, n_y=10$	6.0017e-5	5.3580e-2	1.1461e-1
5.0×10^{-5}	$n_x=60, n_y=20$	5.9238e-5	4.1413e-2	9.6347e-2

https://doi.org/10.4208/cicp.120715.010216a Published online by Cambridge University Press

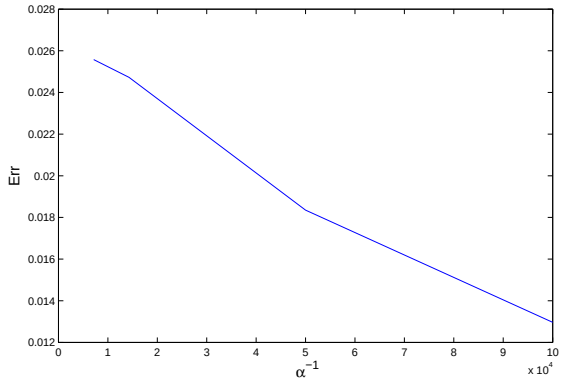


Figure 7: Evolution of the error (L^2-norm) with respect to α^{-1} for the mesh size 30×10.

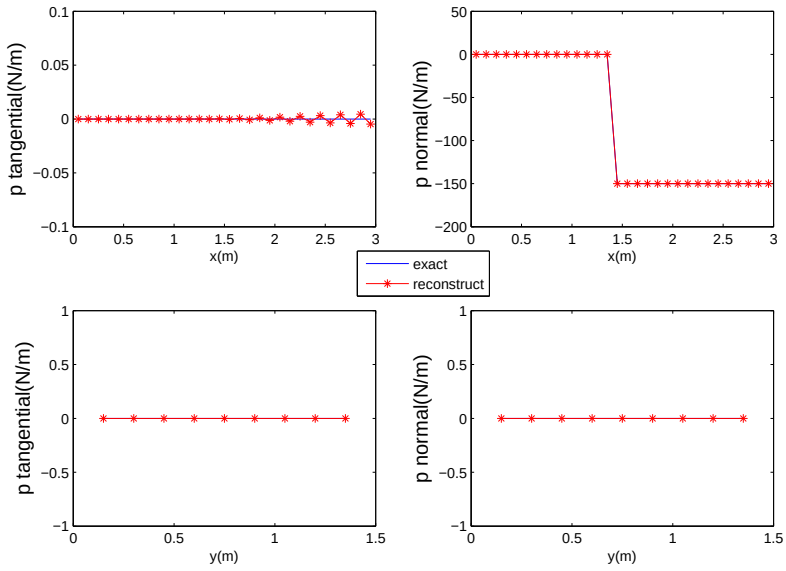


Figure 8: Numerical results based on the observation data $\boldsymbol{u}_d$ in the noise-free case. The mesh size is 30×10. The blue solid line means the exact solution $\mathbf{p}$ (6.3), while the red line with starts is the numerical solution $\mathbf{p}_\alpha^h$. Top row: on the boundary $[0,\ L_1]\times\{L_2\}$. Bottom row: on the boundary $\{L_1\}\times(0,\ L_2)$. Left column: in tangential direction. Right column: in normal direction.

In Fig. 10, we consider the case of the observation data $\boldsymbol{u}_d$ with 2% noise. The first and the second major oscillations locate at the non-smooth positions of $\boldsymbol{p}$, which is the same as the case of no-contacting in Example 6.1. However, comparing with Fig. 5, we may find that the recovery $\boldsymbol{p}_\alpha^h$ in Example 6.2 has a violent period of oscillation. Moreover, from part (b) of Fig. 10, we note that the amplitudes of oscillation increase in the fine mesh and are lager than that in coarse mesh. These can be evidently observed in

https://doi.org/10.4208/cicp.120715.010216a Published online by Cambridge University Press

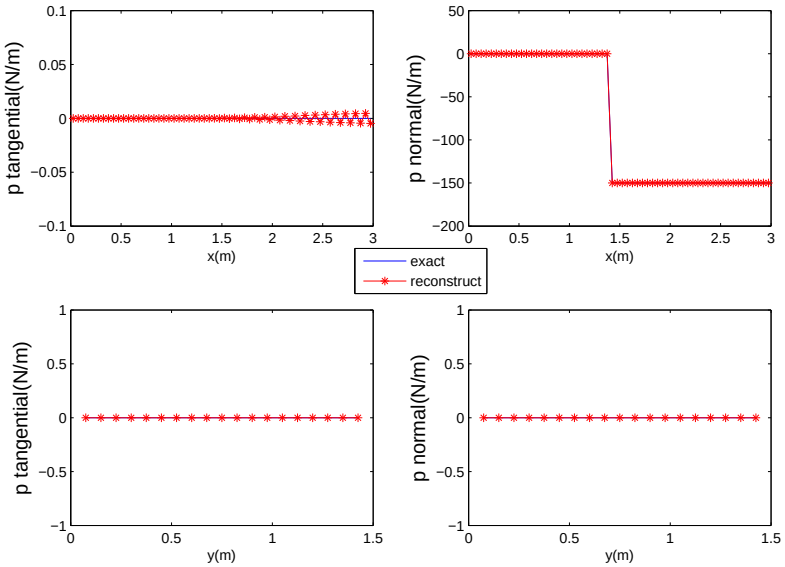
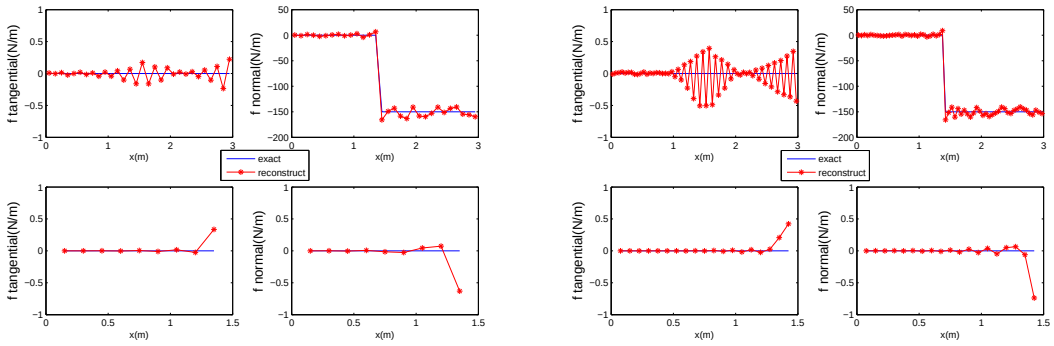


Figure 9: Numerical results based on the observation data $\boldsymbol{u}_d$ in the noise-free case. The mesh size is 60×20. The blue solid line means the exact solution $\mathbf{p}$ (6.3), while the red line with starts is the numerical solution $\mathbf{p}_\alpha^h$. Top row: on the boundary $[0,\ L_1]\times\{L_2\}$. Bottom row: on the boundary $\{L_1\}\times(0,\ L_2)$. Left column: in tangential direction. Right column: in normal direction.

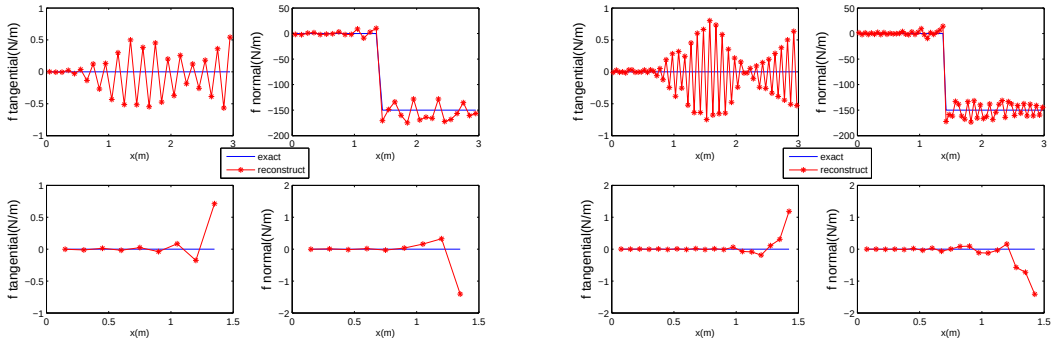


(a) 2% noise in coarse mesh (b) 2% noise in refinement mesh

Figure 10: Numerical results based on the observation data $\boldsymbol{u}_d$ with 2% noise. The blue solid line means the exact solution $\mathbf{p}$ (6.3), while the red line with starts is the numerical solution $\mathbf{p}_\alpha^h$. Top row: on the boundary $[0,\ L_1]\times\{L_2\}$. Bottom row: on the boundary $\{L_1\}\times(0,\ L_2)$. Left column: in tangential direction. Right column: in normal direction.

Fig. 11, the 5% noise case. Factually, in the contacting case, the rigid foundation always produces a reaction force, which influences the displacement of the body severely and increases the difficulty in recovering $\boldsymbol{p}$. Moreover, during the implement of Algorithm

https://doi.org/10.4208/cicp.120715.010216a Published online by Cambridge University Press



(a) 5% noise in coarse mesh (b) 5% noise in refinement mesh

Figure 11: Numerical results based on the observation data $\boldsymbol{u}_d$ with 5% noise. The blue solid line means the exact solution $\mathbf{p}$ (6.3), while the red line with starts is the numerical solution $\mathbf{p}_\alpha^h$. Top row: on the boundary $[0,\ L_1]\times\{L_2\}$. Bottom row: on the boundary $\{L_1\}\times(0,\ L_2)$. Left column: in tangential direction. Right column: in normal direction.

6.1, the contacting case needs more iterations to satisfy the same stop criterion than the no-contacting case (see Fig. 14).

Example 6.3. The exact traction is

$$\mathbf{p}=\begin{cases}\mathbf{0}, & (0,\ L_1/2)\times\{L_2\},\\ (20,-150), & [L_1/2,\ L_1]\times\{L_2\},\\ \mathbf{0}, & \{L_1\}\times(0,\ L_2).\end{cases} \tag{6.4}$$

The top sub-graph of Fig. 12 shows the profile of $\boldsymbol{p}$ (6.4). The first component of $\boldsymbol{p}$ is non-zero, which is different with Example 6.2. In the noise-free case, recovered numerical solution is close to the exact solution. In the 2% noise case Fig. 13, the violent oscillations almost occur at the non-smoothness positions of both the tangential and the normal components of $\boldsymbol{p}$. Particularly, compared with the right-bottom sub-graph of Fig. 10, the oscillations in the right-bottom sub-graph of Fig. 13 obviously have the big amplitudes. The reason may be that the non-zero tangential traction on $[0,\ L_1]\times\{L_2\}$ affects the recovery of the normal component of $\boldsymbol{p}$ on $\{L_1\}\times(0,\ L_2)$.

7 Conclusions

In this paper, we present a mathematical model of the inverse elastic problem and perform a detail mathematical analysis of the corresponding inverse problem. We introduce Tikhonov regularization and the dual problem to prove the uniqueness of the solution of the inverse elastic problem. Moreover, we characterize the solution by an inequality in order to propose a feasible and effective algorithm. We choose three examples for the

https://doi.org/10.4208/cicp.120715.010216a Published online by Cambridge University Press

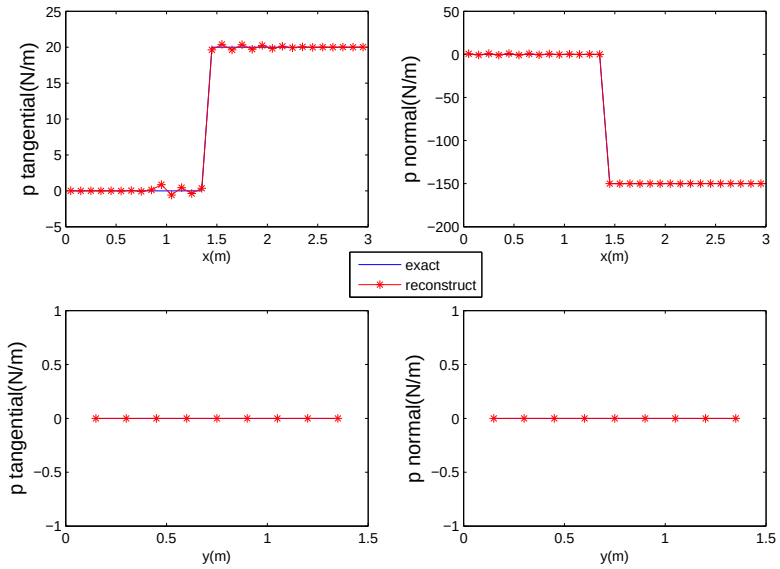


Figure 12: Numerical results based on the observation data $\boldsymbol{u}_d$ in noise-free case.The mesh size is 30×10. The blue solid line means the exact solution $\mathbf{p}$ (6.4), while the red line with starts is the numerical solution $\mathbf{p}_\alpha^h$. Top row: on the boundary $[0,\ L_1]\times\{L_2\}$. Bottom row: on the boundary $\{L_1\}\times(0,\ L_2)$. Left column: in tangential direction. Right column: in normal direction.

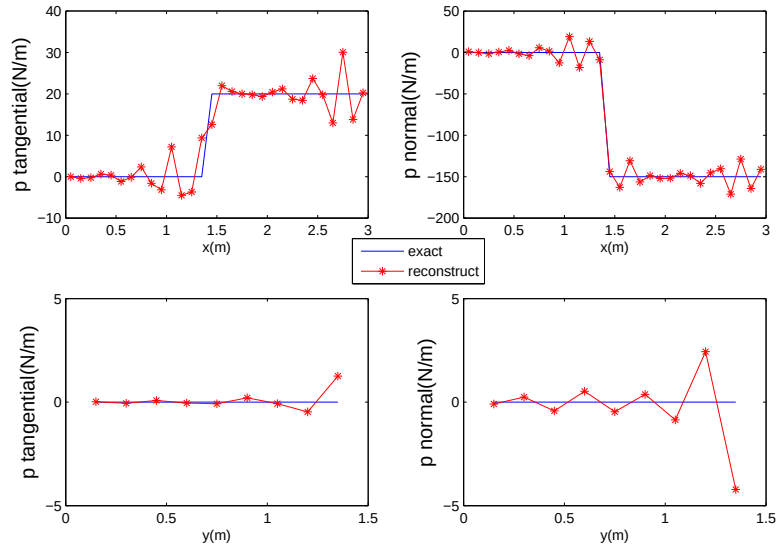


Figure 13: Numerical results based on the observation data $\boldsymbol{u}_d$ with 2% noise. The mesh size is 30×10. The blue solid line means the exact solution $\mathbf{p}$ (6.4), while the red line with starts is the numerical solution $\mathbf{p}_\alpha^h$. Top row: on the boundary $[0,\ L_1]\times\{L_2\}$. Bottom row: on the boundary $\{L_1\}\times(0,\ L_2)$. Left column: in tangential direction. Right column: in normal direction.

https://doi.org/10.4208/cicp.120715.010216a Published online by Cambridge University Press

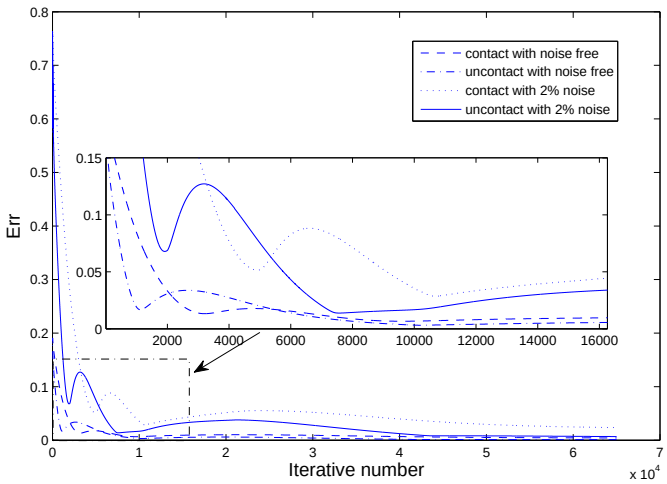


Figure 14: the relative error of two tests without noise.

recovery of different tractions. The tractions may lead the elastic body into two equilibrium states: contacting and not contacting with the rigid obstacle. Moreover, the tractions are non-smooth and discontinuous. Further, we consider three cases of the observation data: noise-free, 2% noise and 5% noise. The recovery numerical results show the efficiency and viability of our algorithm. Of course, the noise causes the oscillations in the recovery numerical solution. The violent oscillations occur at the non-smoothness and the discontinuousness positions of the exact solution. Since our algorithm couples with level-set method, it needs more iterations to satisfy the stop criterion. Especially, in the case of contacting with the rigid obstacle, the algorithm spends more time in level-set method. The main reason is that we can not effectively utilize the reaction force of the rigid foundation.

Acknowledgments

The authors would like to thank the editor and anonymous referees for their valuable comments and suggestions that lead to an improvement of the paper. The work was supported by the Project of NSFC (grant No. 11271258, No. 11471253 and No. 11571311).

References

[1] K. Atkinson and W. Han, *Theoretical Numerical Analysis: A Functional Analysis Framework 3rd edn*, Springer, New York, 2009.
[2] J.V. Beck, B. Blackwell and C.R.St. Clair, *Inverse Heat Conduction: Ill-Posed Problems*, Wiley-Interscience, New York, 1985.

https://doi.org/10.4208/cicp.120715.010216a Published online by Cambridge University Press

[3] A. Bermudez and C. Saguez, Optimal control of a Signorini problem, *SIAM Journal on Control and Optimization*, **25**(1987), 576-582.
[4] H.R. Busby and D.M. Trujillo, Numerical solution to a two-dimensional inverse heat conduction problem, *Int. J. Numer. Meth. Eng.* **21**(1985), 349-359.
[5] W. Chiou, C. Chen and W. Lu, The Inverse Numerical Solutions of the Nonlinear Heat Transfer Problem in Electrical Discharge Machining, *Numerical Heat Transfer, Part A: Applications* **59**(2011), 247-266.
[6] C. Eck, J. Jarušek and M. Krbeč, *Unilateral Contact Problems: Variational Methods and Existence Theorems*, Chapman/CRC Press, New York, 2005.
[7] K. Glashoff and S.A. Gustafson, *Linear Optimization and Approximation: An Introduction to the Theoretical Analysis and Numerical Treatment of Semi-infinite Programs*, Springer, New York, 1983.
[8] K. Grysa, M.J. Cialkowksi and H. Kaminski, An inverse temperature field problem of the theory of thermal stresses, *Nucl. Eng. Des.* **64**(1981), 169-184.
[9] W. Han, *A Posteriori Error Analysis Via Duality Theory: With Applications in Modeling and Numerical Approximations*, Springer, New York, 2005.
[10] W. Han and M. Sofonea, *Quasistatic Contact Problems in Viscoelasticity and Viscoplasticity*, American Mathematical Society–International Press, 2002.
[11] C. Huang and W. Shih, An inverse problem in estimating interfacial cracks in bimaterials by boundary element technique, *Int. J. Numer. Meth. Eng.* **45**(1999), 1547-1567.
[12] V. Isakov, *Inverse Problems for Partial Differential Equations 2nd edn*, Springer, New York, 2006.
[13] J. Kaipio and E. Somersalo, *Statistical and Computational Inverse Problems*, Springer, New York, 2005.
[14] N. Kikuchi and J.T. Oden, *Contact Problems in Elasticity: A Study of Variational Inequalities and Finite Element Methods*, PA: SIAM, Philadelphia, 1998.
[15] A. Maniatty, N. Zabaras and K. Stelson, Finite element analysis of some inverse elasticity problems, *J. Eng. Mech. Diu. ASCE* **115**(1989), 1302-1316.
[16] A. Maniatty and N. Zabaras, A method for solving inverse elastoviscoplastic problems, *J. Eng. Mech. Dio. ASCE* **115**(1989), 2216-2231.
[17] T. Mura, A new NDT: Evaluation of plastic strains in bulk from displacements on surfaces, *Mech. Res. Commun.* **12**(1985), 243-248.
[18] T. Mura, B. Cox and Z. Gao, Computer-aided nondestructive measurements of plastic strains from surface displacements, *Computational Mechanics'86, Vol.I*, Springer-Verlag, New York, 1986.
[19] A.A. Samarskii and P.N. Vabishchevich, *Numerical Methods for Solving Inverse Problems of Mathematical Physics*, Walter de Gruyter, Berlin, 2007.
[20] D.S. Schnur and N. Zabaras, Finite element solution of two-dimensional inverse elastic problems using spatial smoothing, *Int. J. Numer. Meth. Eng.* **30**(1990), 57-75.
[21] M. Shillor, M. Sofonea and J. Telega, *Models and Variational Analysis of Quasistatic Contact*, Springer, Berlin, 2004.
[22] M. Sofonea and A. Matei, *Mathematical Models in Contact Mechanics*, Cambridge University Press, Cambridge, 2012.
[23] A. Tichonov and V. Arsenin, *Solution of ill-Posed Problems*, John Wiley, New York, 1977.
[24] F. Wang, W. Han and X. Cheng, Discontinuous Galerkin methods for solving Signorini problem, *IMA J. Numer. Anal.* **31**(2011), 1754-1772.
[25] E. Zeidler, *Nonlinear Functional Analysis and Its Applications III. Variational Methods and Optimizations*, Springer-Verlag, New York, 1985.

https://doi.org/10.4208/cicp.120715.010216a Published online by Cambridge University Press